

# Electronic Structure of Ligand-Bridged Complexes Containing the $[\text{Rh}_2]^{3+}$ Core: ESR Spectroscopy, MO Calculations, and X-ray Structures of the Three Redox Pairs $[\text{Rh}_2(\text{CO})_2\text{LL}'\{\mu\text{-PhNC}(\text{Me})\text{NPh}\}_2]^z$ [ $z = 0, 1$ ; $\text{L} = \text{L}' = \text{PPh}_3, \text{P}(\text{OPh})_3$ ; $\text{L} = \text{PPh}_3, \text{L}' = \text{P}(\text{OPh})_3$ ]

David C. Boyd,<sup>†</sup> Neil G. Connelly,<sup>\*,‡</sup> Gabriel Garcia Herbosa,<sup>‡</sup> Michael G. Hill,<sup>†</sup> Kent R. Mann,<sup>†</sup> Carlo Mealli,<sup>§</sup> A. Guy Orpen,<sup>‡</sup> Karen E. Richardson,<sup>‡</sup> and Philip H. Rieger<sup>||</sup>

School of Chemistry, University of Bristol, Bristol BS8 1TS, U.K., Department of Chemistry, Brown University, Providence, Rhode Island 02912, Department of Chemistry, University of Minnesota, Minneapolis, Minnesota 55455, and Istituto per lo Studio della Stereochimica ed Energetica dei Composti di Coordinazione, CNR, I-50132 Firenze, Italy

Received November 5, 1993<sup>⊙</sup>

The X-ray crystal structure analyses of the three redox pairs  $[\text{Rh}_2(\text{CO})_2\text{LL}'\{\mu\text{-PhNC}(\text{Me})\text{NPh}\}_2]^z$  [ $z = 0, 1$ ;  $\text{L} = \text{L}' = \text{PPh}_3$  (1, 1<sup>+</sup>);  $\text{L} = \text{L}' = \text{P}(\text{OPh})_3$  (2, 2<sup>+</sup>);  $\text{L} = \text{PPh}_3, \text{L}' = \text{P}(\text{OPh})_3$  (3, 3<sup>+</sup>)] are reported and the molecular structures compared with those of  $[\text{Rh}_2(\text{CO})_2(\text{PPh}_3)_2(\mu\text{-RNNNR})_2]^z$  [ $z = 0, 1$ ;  $\text{R} = p\text{-tolyl}$  (4, 4<sup>+</sup>)]. These complexes have locally planar rhodium coordination with the planes splayed apart between 20 and 40°. The nonbonded Rh...Rh distance of ca. 2.9 Å in the neutral complexes is reduced by between 0.147(2) and 0.262(4) Å on oxidation. These and other changes in the molecular structure are consistent with the HOMO of the neutral complexes being delocalized, over the two metals, and having rhodium–rhodium  $\sigma^*$  character. ESR spectroscopic analysis is reported on 1<sup>+</sup>–4<sup>+</sup> and on the related ligand-bridged  $[\text{Rh}_2]^{3+}$  species  $[\text{Rh}_2(\text{CO})_2(\mu\text{-dppm})(\mu\text{-RNNNR})_2]^+$  [ $\text{R} = p\text{-tolyl}$  (5<sup>+</sup>)],  $[\text{Rh}_2(\mu\text{-dimen})_2(\mu\text{-dppm})_2]^{3+}$  (6<sup>+</sup>, dimen = 1,8-diisocyanomenthane),  $[\text{Rh}_2(\mu\text{-TM4})_2(\mu\text{-dppm})_2]^{3+}$  [TM4 = 2,5-diisocyno-2,5-dimethylhexane (7<sup>+</sup>)],  $[\text{Rh}_2(\mu\text{-CNCH}_2\text{CH}_2\text{CH}_2\text{NC})(\mu\text{-dppm})_2]^{3+}$  (8<sup>+</sup>),  $[\text{Rh}_2(\mu\text{-HTP5})_2(\mu\text{-dppm})_2]^{3+}$  (9<sup>+</sup>, HTP5 = 1,5-diisocyno-1,1,5-triphenylpentane),  $[\text{Rh}_2(\text{CO})_2(\text{PMe}_2\text{Ph})_2(\mu\text{-chp})_2]^+$  (10<sup>+</sup>),  $[\text{Rh}_2(\mu\text{-mhp})_2(\text{COD})_2]^+$  (11<sup>+</sup>),  $[\text{Rh}_2(\mu\text{-chp})_2(\text{NBD})_2]^+$  (12<sup>+</sup>), and  $[\text{Rh}_2(\mu\text{-mhp})_2(\text{NBD})_2]^+$  (13<sup>+</sup>). The spectroscopic parameters are shown to be dependent on the geometry of the cations and especially on the splay angle between the rhodium coordination planes. Quantitative interpretation of the ESR parameters suggests an orbital composition for the SOMO which is in good agreement with extended Hückel MO calculations on the model compounds  $[\{\text{Rh}(\text{H})_2(\text{CO})_2\}_2]^{2-}$  (14) and  $[\text{Rh}_2(\text{CO})_4(\mu\text{-HNNNH})_2]$  (15). The theoretical and ESR analyses are in full accord with the X-ray results and together provide a coherent picture of the electronic and geometric structures of ligand-bridged  $[\text{Rh}_2]^{3+}$  complexes.

## Introduction

As a well-defined oxidation state in mononuclear chemistry, Rh(II) is relatively rare,<sup>1</sup> though recent studies suggest a rich chemistry for complexes such as  $[\text{Rh}(\text{tmpp})_2]^{2+}$  [tmpp = tris-(2,4,6-trimethoxyphenyl)phosphine],<sup>2a,b</sup>  $[\text{Rh}(\text{tetramesitylporphyrin})]^{2c}$  and  $[\text{Rh}(\text{C}\equiv\text{CR})\text{L}]^+$  [ $\text{L} = \text{E}(\text{CH}_2\text{CH}_2\text{PPh}_2)_3$ ;  $\text{E} = \text{N}, \text{P}$ ].<sup>2d,e</sup> By contrast, divalent rhodium is commonly to be found<sup>3</sup> in binuclear species with  $[\text{Rh}_2]^{4+}$  (formally  $\text{Rh}^{\text{II}}\text{Rh}^{\text{II}}$ ) and  $[\text{Rh}_2]^{5+}$  (formally  $\text{Rh}^{\text{II}}\text{Rh}^{\text{III}}$ ) cores. The electronic structures of “face-to-face” tetrabridged binuclear complexes with  $[\text{Rh}_2]^{4+}$  and  $[\text{Rh}_2]^{5+}$  cores, namely  $[\text{Rh}_2(\mu\text{-L})_4]^z$  ( $z = 0, 1$ ;  $\text{L} = \text{O}, \text{O}^-, \text{O}, \text{N}^-, \text{N}, \text{S}^-, \text{N}, \text{N}$ -donor, etc.), have been studied<sup>4–7</sup> in considerable detail, often by a combination of theory<sup>4b,5,6</sup> with electrochemistry<sup>4</sup> and ESR spectroscopy.<sup>4b,d,f,h,6</sup> The electronic configuration of the

$[\text{Rh}_2]^{4+}$  state is generally accepted<sup>8</sup> to be  $\sigma^2\pi^4\delta^2\delta^*\pi^*4$  whereas that of  $[\text{Rh}_2]^{5+}$  is dependent on the nature of the bridging ligands and on the type and number of ligands bound to the axial sites. For example, the unpaired electrons of  $[\text{Rh}_2(\mu\text{-acetate})_4\text{L}_2]^+$  ( $\text{L} = \text{H}_2\text{O}, \text{MeCN}, \text{acetone}, \text{etc.}$ ),  $[\text{Rh}_2(\mu\text{-O}_2\text{CR})_4\text{L}_2]^+$  ( $\text{R} = \text{Et}, \text{CF}_3$ ;  $\text{L} = \text{phosphine}, \text{phosphite}$ ), and  $[\text{Rh}_2(\mu\text{-acetate})_{4-n}\{\mu\text{-CH}_3\text{C}(\text{O})\text{NH}\}_n(\text{NCMe})_2]^+$  ( $n = 1\text{--}4$ ) occupy metal–metal orbitals with  $\pi^*$ ,  $\sigma$ , and  $\delta^*$  symmetry, respectively;<sup>6</sup> axial coordination can also lead to localization of the unpaired electron on one metal atom, as in  $[\text{Rh}_2(\mu\text{-ap})_4\text{Cl}]$  ( $\text{ap} = 2\text{-anilinopyridinate}$ ).<sup>4g</sup>

In contrast to the higher oxidation states, the electronic structure

<sup>†</sup> University of Minnesota.

<sup>‡</sup> University of Bristol.

<sup>§</sup> CNR Firenze.

<sup>||</sup> Brown University.

<sup>⊙</sup> Abstract published in *Advance ACS Abstracts*, January 15, 1994.

- (a) Hay-Motherwell, R. S.; Koschmieder, S. U.; Wilkinson, G.; Hussain-Bates, B.; Hursthouse, M. B. *J. Chem. Soc., Dalton Trans.* **1991**, 2821–2830. (b) Ogle, C. A.; Masterman, T. C.; Hubbard, J. L. *J. Chem. Soc., Chem. Commun.* **1990**, 1733–1734.
- (a) Haefner, S. C.; Dunbar, K. R.; Bender, C. J. *Am. Chem. Soc.* **1991**, *113*, 9540–9553. (b) Dunbar, K. R.; Haefner, S. C. *Organometallics* **1992**, *11*, 1431–1433. (c) Wayland, B. B.; Ba, S.; Sherry, A. E. *J. Am. Chem. Soc.* **1991**, *113*, 5305–5311. (d) Bianchini, C.; Meli, A.; Peruzzini, M.; Vacca, A.; Zanella, P.; Ottaviani, F. M. *Organometallics* **1990**, *9*, 241–250. (e) Bianchini, C.; Meli, A.; Peruzzini, M.; Zanobini, F.; Zanella, P. *Organometallics* **1990**, *9*, 360–371.
- (a) Felthouse, T. R. *Prog. Inorg. Chem.* **1982**, *29*, 73–166. Cotton, F. A.; Walton, R. A. *Multiple Bonds Between Metal Atoms*; Wiley-Interscience: New York, 1982; Chapter 7.

- (4) See, for example: (a) Herbert, J. W.; Macartney, D. H. *Inorg. Chem.* **1985**, *24*, 4398–4402. (b) Chavan, M. Y.; Zhu, T. P.; Lin, X. Q.; Ahsan, M. Q.; Bear, J. L.; Kadish, K. M. *Inorg. Chem.* **1984**, *23*, 4538–4545. (c) Bear, J. L.; Zhu, T. P.; Malinski, T.; Dennis, A. M.; Kadish, K. M. *Inorg. Chem.* **1985**, *24*, 674–678. (d) Le, J. C.; Chavan, M. Y.; Chau, L. K.; Bear, J. L.; Kadish, K. M. *J. Am. Chem. Soc.* **1985**, *107*, 7195–7197. (e) Tocher, D. A.; Tocher, J. H. *Inorg. Chim. Acta* **1985**, *104*, L15–L17. (f) Bear, J. L.; Lifsey, R. S.; Chau, L. K.; Ahsan, M. Q.; Korp, J. D.; Chavan, M.; Kadish, K. M. *J. Chem. Soc., Dalton Trans.* **1989**, 93–100. (g) Bear, J. L.; Yao, C.-L.; Liu, F. J.; Capdevielle, F. J.; Korp, J. D.; Albright, T. A.; Kang, S.-K.; Kadish, K. M. *Inorg. Chem.* **1989**, *28*, 1254–1262. (h) Lifsey, R. S.; Chavan, M. Y.; Chau, L. K.; Ahsan, M. Q.; Kadish, K. M.; Bear, J. L. *Inorg. Chem.* **1987**, *26*, 822–829. (i) Piraino, P.; Bruno, G.; Schiavo, S. L.; Laschi, F.; Zanella, P. *Inorg. Chem.* **1987**, *26*, 2205–2211.
- (5) Poblet, J. M.; Benard, M. *Inorg. Chem.* **1988**, *27*, 2935–2941.
- (6) (a) Kawamura, T.; Katayama, H.; Nishikawa, H.; Yamabe, T. *J. Am. Chem. Soc.* **1989**, *111*, 8156–8160. (b) Kawamura, T.; Jukamachi, K.; Sowa, T.; Hayashida, S.; Yonezama, T. *J. Am. Chem. Soc.* **1981**, *103*, 364–369.
- (7) Best, S. P.; Clark, R. J. H.; Nightingale, A. J. *Inorg. Chem.* **1990**, *29*, 1383–1387.
- (8) Wheeler, R. A.; Piela, L.; Hoffmann, R. *J. Am. Chem. Soc.* **1988**, *110*, 7302–7315.

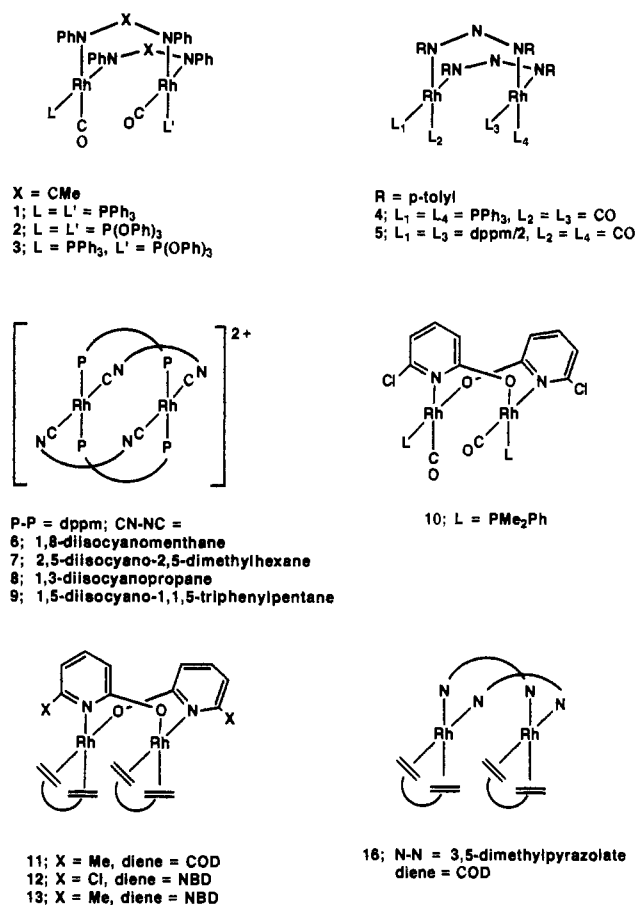
of  $[Rh_2]^{3+}$  (formally  $Rh^I Rh^{II}$ ) is poorly defined. In part this is due to the difficulty with which the  $[Rh_2]^{4+}$  core of tetrabridged complexes can be reduced, though the anions  $[Rh_2(\mu\text{-carboxylate})_4]^-$  and  $[Rh_2(\mu\text{-PhNCPPhNPh})_4]^-$  have been generated by  $^{60}Co\gamma$ -irradiation of  $[Rh_2(\mu\text{-carboxylate})_4]^9$  and electrochemical reduction of  $[Rh_2(\mu\text{-PhNCPPhNPh})_4]^{4d}$  respectively; the ESR spectra suggest that the unpaired electron occupies a  $\sigma^*$  orbital. However, it is becoming apparent that the  $[Rh_2]^{3+}$  core can be stabilized when the dirhodium unit is associated with  $\pi$ -bonding ligands such as CO, isocyanides, or unsaturated hydrocarbons.<sup>10</sup> We, for example, have described the synthesis and electrochemistry of a wide range of  $[Rh_2]^{3+}$  complexes derived from the triazenide- and acetamidino-bridged complexes  $[Rh_2(CO)_4(\mu\text{-RNXNR})_2]$  ( $X = N$ ,  $R = p\text{-tolyl}$ ;  $X = CMe$ ,  $R = Ph$ )<sup>11</sup> and the 2-hydroxypyridinate-bridged complexes  $[Rh_2(\mu\text{-L-L}')_2(\text{diene})_2]$  [ $L-L' = 6\text{-chloro-2-hydroxypyridinate (chp)}$ ,  $6\text{-methyl-2-hydroxypyridinate (mhp)}$ ; diene = norbornadiene (NBD), 1,5-cyclooctadiene (COD)].<sup>12</sup>

Our preliminary work<sup>11c</sup> showed that the bonding in  $[Rh_2]^{3+}$  complexes such as  $[Rh_2(CO)_2(PPh_3)_2(\mu\text{-RNNNR})_2]^+$  is most likely delocalized, with the unpaired electron occupying an antibonding orbital comprising the out-of-phase combination of the  $4d_z^2$  orbitals on each of the two rhodium atoms. We now present a more detailed study of electronic structure involving the following: (i) the X-ray crystal structures of the four redox pairs  $[Rh_2(CO)_2LL'\{\mu\text{-PhNC(Me)NPh}\}_2]$  [ $z = 0, 1$ ;  $L = L' = PPh_3$  (**1**,  $1^+$ );  $L = L' = P(OPh)_3$  (**2**,  $2^+$ );  $L = PPh_3$ ,  $L' = P(OPh)_3$  (**3**,  $3^+$ )] and  $[Rh_2(CO)_2(PPh_3)_2(\mu\text{-RNNNR})_2]^z$  [ $z = 0, 1$ ;  $R = p\text{-tolyl}$  (**4**,  $4^+$ );<sup>11c</sup> (ii) an ESR spectroscopic analysis of these and several other  $[Rh_2]^{3+}$ -containing complexes, namely  $[Rh_2(CO)_2(\mu\text{-dppm})(\mu\text{-RNNNR})_2]^+$  [ $R = p\text{-tolyl}$  (**5**<sup>+</sup>)],  $[Rh_2(\mu\text{-dimen})_2(\mu\text{-dppm})_2]^{3+}$  (**6**<sup>+</sup>, dimen = 1,8-diisocyanomenthane),<sup>13</sup>  $[Rh_2(\mu\text{-TM4})_2(\mu\text{-dppm})_2]^{3+}$  [ $TM4 = 2,5\text{-diisocyno-2,5-dimethylhexane}$  (**7**<sup>+</sup>)],  $[Rh_2(\mu\text{-CNCH}_2\text{CH}_2\text{CH}_2\text{NC})_2(\mu\text{-dppm})_2]^{3+}$  (**8**<sup>+</sup>),  $[Rh_2(\mu\text{-HTP5})_2(\mu\text{-dppm})_2]^{3+}$  (**9**<sup>+</sup>, HTP5 = 1,5-diisocyno-1,1,5-triphenylpentane),  $[Rh_2(CO)_2(PMe_2Ph)_2(\mu\text{-chp})_2]^+$  (**10**<sup>+</sup>),  $[Rh_2(\mu\text{-mhp})_2(\text{COD})_2]^+$  (**11**<sup>+</sup>),  $[Rh_2(\mu\text{-chp})_2(\text{NBD})_2]^+$  (**12**<sup>+</sup>), and  $[Rh_2(\mu\text{-mhp})_2(\text{NBD})_2]^+$  (**13**<sup>+</sup>); (iii) extended Hückel MO calculations on the model compounds  $[\text{Rh}(\text{H})_2(\text{CO})_2]^{2-}$  (**14**) and  $[Rh_2(CO)_4(\mu\text{-HNNNH})_2]$  (**15**). These complexes are shown in Chart 1.

## Experimental Section

The preparation, purification, and reactions of the complexes described were carried out under an atmosphere of dry nitrogen using dried, distilled, and deoxygenated solvents. Purification was achieved by dissolving the complex in an appropriate solvent, filtering the solution through Celite, adding a solvent in which the product is insoluble, and reducing the solvent

Chart 1. Complexes 1–13 and 16



volume *in vacuo* to induce precipitation. Unless stated otherwise, the complexes are air-stable in the solid state and dissolve in polar solvents such as  $CH_2Cl_2$ , acetone, or thf to give solutions which only slowly decompose in air. Infrared spectra were recorded on Nicolet MX5 or 5ZDX and Mattson Sirius 100 or Galaxy 6021 FT spectrometers,  $^1H$  NMR spectra on a Nicolet NT-300WB spectrometer, and UV-visible spectra on Cary 17D or Tracor Northern TN-6500 rapid scan spectrophotometers. ESR spectra of frozen THF/ $CH_2Cl_2$  (2:1) solutions of  $1^+ - 5^+$  were obtained at 77 K using a Varian V-4502 spectrometer at the University of Bristol. Solutions of  $6^+ - 13^+$  were generated by bulk electrolysis of  $ca. 5 \times 10^{-4}$  mol  $dm^{-3}$  solutions of compounds **6–13** in  $CH_2Cl_2$  containing 0.1 mol  $dm^{-3}$   $[NBu_4][ClO_4]$ . ESR spectra of the frozen solutions of  $6^+ - 13^+$  were obtained at 100–140 K at the University of Minnesota using a Varian E-3 or a Bruker ESP300 spectrometer equipped with a variable-temperature controller. All ESR spectra were calibrated using the diphenylpicrylhydrazyl (dpph) radical as an internal *g*-value standard. Microanalyses were carried out by the staff of the Microanalytical Service of the School of Chemistry, University of Bristol, or by MHW Laboratories, Phoenix, AZ.

The complexes **1**, **3**, and **4**,  $1^+$ ,  $3^+$ ,  $4^+$ , and **5**<sup>+</sup> (as the hexafluorophosphate salts),<sup>11d</sup> and **9**, **11**, and **12**<sup>12e,d,c</sup> were prepared by published methods; compounds **6–8** were prepared by a modification of the method of Yaneff and Powell.<sup>14</sup>

$[Rh_2(CO)_2[P(OPh)_3]_2\{\mu\text{-PhNC(Me)NPh}\}_2][PF_6]$  (**2**<sup>+</sup>). To a stirred solution of  $[Rh_2(CO)_4\{\mu\text{-PhNC(Me)NPh}\}_2]$  (0.334 g, 0.45 mmol) in  $CH_2Cl_2$  (40  $cm^3$ ) was added  $P(OPh)_3$  (0.28 g, 0.90 mmol) followed by  $[FeCp_2][PF_6]$  (0.15 g, 0.45 mmol). The solution immediately changed from red to brown with rapid evolution of CO. After 10 min, filtration of the solution through Celite, addition of *n*-hexane (50  $cm^3$ ), and reduction of the solvent volume *in vacuo* gave a brown oily solid. The orange ferrocene-containing mother liquors were discarded, and purification from thf-*n*-hexane afforded a brown powder, yield 0.55 g (84%). IR ( $CH_2Cl_2$ ): 2063 and 2043  $cm^{-1}$ . Anal. Calcd for  $C_{66}H_{56}N_4O_8F_6Rh_2$ : C, 54.8; H, 3.9; N, 3.9. Found: C, 55.2; H, 4.1; N, 4.0.

$[Rh_2(CO)_2[P(OPh)_3]_2\{\mu\text{-PhNC(Me)NPh}\}_2]$  (**2**). To a stirred solution of  $[Rh_2(CO)_2[P(OPh)_3]_2\{\mu\text{-PhNC(Me)NPh}\}_2][PF_6]$  (0.40 g, 0.28 mmol)

- (9) (a) Eastland, G. W.; Symons, M. C. R. *J. Chem. Soc., Dalton Trans.* **1984**, 2193–2196. (b) Pruchnik, F.; Jezierski, A.; Kalcinska, E. *Polyhedron* **1991**, *10*, 2551–2557.
- (10) (a) Hill, M. G.; Mann, K. R. *Inorg. Chem.* **1991**, *30*, 1429–1431. (b) Fjeldsted, D. O. K.; Stobart, S. R. *J. Chem. Soc., Chem. Commun.* **1985**, 908–909. (c) Connelly, N. G.; Loyns, A. C.; Fernandez, M. J.; Modrego, J.; Oro, L. A. *J. Chem. Soc., Dalton Trans.* **1989**, 683–687. (d) Beveridge, K. A.; Bushnell, G. W.; Stobart, S. R.; Atwood, J. L.; Zaworotko, M. J. *Organometallics* **1983**, *2*, 1447–1451.
- (11) (a) Connelly, N. G.; Loyns, A. C. *J. Organomet. Chem.* **1991**, *411*, 285–290. (b) Brauns, T.; Carriedo, C.; Cockayne, J. S.; Connelly, N. G.; Garcia Herbosa, G.; Orpen, A. G. *J. Chem. Soc., Dalton Trans.* **1989**, 2049–2059. (c) Connelly, N. G.; Garcia Herbosa, G. *J. Chem. Soc., Chem. Commun.* **1987**, 246–248. (d) Connelly, N. G.; Garcia, G.; Gilbert, M.; Stirling, J. S. *J. Chem. Soc., Dalton Trans.* **1987**, 1403–1408. (e) Connelly, N. G.; Finn, C. J.; Freeman, M. J.; Orpen, A. G.; Stirling, J. S. *J. Chem. Soc., Chem. Commun.* **1984**, 1025–1027.
- (12) (a) Miskowski, V. M.; Sigal, I. S.; Mann, K. R.; Gray, H. B.; Milder, S. J.; Hammond, G. S.; Ryason, P. R. *J. Am. Chem. Soc.* **1979**, *101*, 4383–4385. (b) Boyd, D. C.; Matsch, P. A.; Mixa, M. M.; Mann, K. R. *Inorg. Chem.* **1986**, *25*, 3331–3333. (c) Boyd, D. C.; Szalapski, R.; Mann, K. R. *Organometallics* **1989**, *8*, 790–795. (d) Rodman, G. S.; Mann, K. R. *Inorg. Chem.* **1988**, *27*, 3338–3346. (e) Daws, C. A.; Hill, M. G.; Bullock, J. P.; Mann, K. R. *Inorg. Chem.*, in press.
- (13) Spectra of  $6^+$ ,  $9^+$ , and  $12^+$  have been reported previously<sup>12b,c,e</sup> but have been reinterpreted for this paper.

- (14) Yaneff, P. V.; Powell, J. J. *Organomet. Chem.* **1979**, *179*, 101–113. Mixa, M. M. Ph.D. Thesis, University of Minnesota, 1986.

Table 1. Details of Crystal Structure Determinations

	1-C <sub>6</sub> H <sub>14</sub>	1 <sup>+</sup> -PF <sub>6</sub> -2C <sub>6</sub> H <sub>14</sub>	2	2 <sup>+</sup> -PF <sub>6</sub>	3-Et <sub>2</sub> O	3 <sup>+</sup> -PF <sub>6</sub> -CH <sub>2</sub> Cl <sub>2</sub>
empirical formula	C <sub>22</sub> H <sub>30</sub> N <sub>4</sub> O <sub>2</sub> P <sub>2</sub> Rh <sub>2</sub>	C <sub>18</sub> H <sub>24</sub> N <sub>4</sub> O <sub>2</sub> P <sub>3</sub> F <sub>6</sub> Rh <sub>2</sub>	Crystal Data C <sub>66</sub> H <sub>56</sub> N <sub>4</sub> O <sub>4</sub> P <sub>4</sub> Rh <sub>2</sub>	C <sub>66</sub> H <sub>56</sub> N <sub>4</sub> O <sub>4</sub> P <sub>4</sub> F <sub>4</sub> Rh <sub>2</sub>	C <sub>70</sub> H <sub>66</sub> N <sub>4</sub> O <sub>6</sub> P <sub>2</sub> Rh <sub>2</sub>	C <sub>67</sub> H <sub>58</sub> Cl <sub>2</sub> N <sub>4</sub> O <sub>3</sub> P <sub>4</sub> Rh <sub>2</sub>
M <sub>r</sub>	1291.1	1522.2	1300.95	1445.91	1327.08	1368.8
cryst habit	red flat needles	brown, elongated blocks	red flat needles	brown square plates	red blocks	brown flat needles
cryst solvent(s)	toluene- <i>n</i> -hexane	CH <sub>2</sub> Cl <sub>2</sub> - <i>n</i> -hexane	toluene- <i>n</i> -hexane	ethanol at -20 °C	diethyl ether- <i>n</i> -hexane	CH <sub>2</sub> Cl <sub>2</sub> - <i>n</i> -hexane
cryst size (mm)	0.55 × 0.15 × 0.05	0.70 × 0.40 × 0.20	0.80 × 0.50 × 0.35	0.50 × 0.45 × 0.15	0.70 × 0.45 × 0.37	0.60 × 0.40 × 0.13
cryst system	monoclinic	monoclinic	monoclinic	monoclinic	monoclinic	monoclinic
space group	12/a (No. 15)	C2/c (No. 15)	C2/c (No. 15)	P2 <sub>1</sub> /n (No. 14)	P2 <sub>1</sub> /n (No. 14)	P2 <sub>1</sub> /n (No. 14)
unit cell dimens a (Å)	20.239(7)	22.908(6)	21.386(4)	11.904(4)	13.373(6)	14.224(4)
b (Å)	23.961(7)	17.837(4)	18.180(4)	20.786(8)	23.399(8)	24.409(8)
c (Å)	26.256(9)	18.792(8)	15.764(4)	26.290(8)	20.261(7)	19.210(7)
β (deg)	93.8(3)	110.34(3)	100.42(2)	101.13(3)	93.19(3)	94.94(3)
V (Å <sup>3</sup> )	12.705(7)	7200(4)	6028(2)	6383(4)	6330(4)	6645(4)
Z	8	4	4	4	4	4
D(calc) (Mg/m <sup>3</sup> )	1.34	1.25	1.37	1.51	1.39	1.368
abs coeff (mm <sup>-1</sup> )	0.62	0.59	0.66	0.66	0.62	0.71
F(000)	5328	3140	2656	2932	2728	3004
temp (K)	291	291	291	196	291	291
scan type	Wyckoff, ω	Wyckoff, ω	ω/2θ	Wyckoff, ω	Wyckoff, ω	Wyckoff, ω
scan range (ω) (deg)	0.6	0.6	1.2+Δ <sub>det</sub>	1.6	0.6	0.6
scan speed (deg/min in ω)	1.0-14.65	1.0-14.65	0.5-14.65	2.0-14.65	0.8-29.3	1.0-29.3
check reflns	(5,2,11), (0,11,5), (9,4,3)	(3,5,-5), (-7,-3,-4), (-9,3,2)	(-8,-6,8), (3,1,5), (5,-7,3)	(-3,6,-4), (-6,0,10), (-5,1,5)	(3,1,9), (3,10,3), (-6,4,4)	(7,-1,-2), (-5,2,7), (0,12,1)
% variation in above index ranges	5	2	3	2	3	5
no. of reflcns colld	0 ≤ h ≤ 24, 0 ≤ k ≤ 28, -31 ≤ l ≤ 31	0 ≤ h ≤ 27, 0 ≤ k ≤ 21, -22 ≤ l ≤ 22	0 ≤ h ≤ 25, 0 ≤ k ≤ 21, -18 ≤ l ≤ 18	0 ≤ h ≤ 14, 0 ≤ k ≤ 15, -31 ≤ l ≤ 31	0 ≤ h ≤ 16, 0 ≤ k ≤ 28, -25 ≤ l ≤ 25	0 ≤ h ≤ 17, 0 ≤ k ≤ 30, -23 ≤ l ≤ 23
no. of indpt reflns	8621	6686	5686	11 035	11 776	10 371
N <sub>obs</sub>	8104	6302	5344	10 159	10 961	9675
no. of azimuthal scan data	5782	4854	4286	8260	9401	8512
min, max transm coeffs	397	370	420	335	76	396
	0.832, 0.897	0.517, 0.690	0.569, 0.617	0.536, 0.639	0.556, 0.601	0.40, 0.57
no. of least-squares variables	708	417	370	858	757	808
g	0.0005	0.0008	0.00065	0.0005	0.00065	0.00065
non-H atoms	all but solvent	all but solvent	all	all	all	all
thermal params anisotropic	solvent; C(67)-C(72)	solvent; C(49)-C(54)	none	none	none	none
thermal params isotropic	solvent atoms	solvent atoms, F(2-5)	none	none	none	none
disorder, partial occupancy	R = 5.31, R <sub>w</sub> = 4.69	R = 4.85, R <sub>w</sub> = 4.69	R = 3.40, R <sub>w</sub> = 3.33	R = 3.75, R <sub>w</sub> = 3.70	R = 3.40, R <sub>w</sub> = 3.70	R = 4.31, R <sub>w</sub> = 4.45
final R indices (%)	1.133	1.350	1.026	1.285	1.224	1.357
goodness-of-fit, S	0.504, -0.488	0.84, -0.80	0.38, -0.32	0.60, -0.52	0.65, -0.36	0.29, -0.27
E <sub>max</sub> , E <sub>min</sub> (e Å <sup>-3</sup> )						

**Table 2.** Atomic Coordinates ( $\times 10^4$ ) and Equivalent Isotropic Displacement Parameters ( $\text{\AA}^2 \times 10^3$ ) for [Rh<sub>2</sub>(CO)<sub>2</sub>(PPh<sub>3</sub>)<sub>2</sub>( $\mu$ -PhNC(Me)NPh)<sub>2</sub>]-C<sub>6</sub>H<sub>14</sub> (1-C<sub>6</sub>H<sub>14</sub>)

	x	y	z	U(eq) <sup>a</sup>		x	y	z	U(eq) <sup>a</sup>
Rh(1)	1032(1)	4556(1)	3029(1)	37(1)	C(32)	2733(4)	4454(4)	1873(3)	60(4)
Rh(2)	450(1)	3439(1)	3238(1)	38(1)	C(33)	3254(4)	4108(5)	1773(4)	72(4)
P(1)	1463(1)	4647(1)	2255(1)	41(1)	C(34)	3263(5)	3561(5)	1916(4)	69(4)
P(2)	933(1)	2972(1)	3919(1)	47(1)	C(35)	2759(5)	3367(4)	2186(3)	68(4)
N(1)	46(3)	4674(3)	2720(2)	39(2)	C(36)	2240(4)	3699(4)	2300(3)	55(3)
N(2)	-160(3)	3739(3)	2606(2)	41(2)	C(37)	1738(4)	5365(3)	2122(3)	45(3)
N(3)	644(3)	4647(3)	3759(2)	40(2)	C(38)	1717(5)	5577(4)	1637(4)	74(4)
N(4)	-143(3)	3945(3)	3700(2)	43(2)	C(39)	1964(6)	6106(5)	1553(5)	98(6)
O(1)	2394(3)	4494(3)	3507(2)	71(3)	C(40)	2223(6)	6423(5)	1945(6)	92(6)
O(2)	1127(3)	2676(2)	2554(2)	65(2)	C(41)	2244(5)	6219(4)	2422(5)	78(5)
C(1)	1864(4)	4508(3)	3319(3)	45(3)	C(42)	2003(4)	5689(4)	2519(4)	60(4)
C(2)	877(4)	2974(3)	2826(3)	46(3)	C(43)	934(4)	4484(4)	1679(3)	52(3)
C(3)	-339(4)	4260(3)	2526(3)	44(3)	C(44)	381(4)	4809(4)	1555(3)	60(4)
C(4)	109(4)	4416(3)	3926(3)	44(3)	C(45)	-18(5)	4695(5)	1129(4)	84(5)
C(5)	-961(4)	4389(3)	2185(3)	56(3)	C(46)	119(6)	4249(6)	822(4)	112(6)
C(6)	-210(4)	4668(4)	4376(3)	66(4)	C(47)	655(7)	3926(5)	944(4)	117(6)
C(7)	-210(4)	5224(3)	2777(3)	38(3)	C(48)	1070(5)	4046(4)	1366(4)	79(4)
C(8)	-820(4)	5328(3)	2970(3)	52(3)	C(49)	953(5)	3284(4)	4553(3)	64(4)
C(9)	-1028(4)	5869(4)	3056(3)	55(3)	C(50)	1539(6)	3438(4)	4814(4)	85(4)
C(10)	-642(4)	6322(4)	2956(3)	58(4)	C(51)	1555(7)	3675(6)	5301(5)	120(6)
C(11)	-39(4)	6227(3)	2755(3)	52(3)	C(52)	991(10)	3759(6)	5519(5)	146(8)
C(12)	171(4)	5685(3)	2671(3)	48(3)	C(53)	404(8)	3618(7)	5275(5)	155(9)
C(13)	-492(5)	3302(3)	2327(4)	54(3)	C(54)	378(6)	3388(5)	4792(4)	102(5)
C(14)	-1034(5)	3046(4)	2494(4)	79(4)	C(55)	515(4)	2308(4)	4013(3)	55(3)
C(15)	-1344(7)	2604(5)	2234(6)	110(6)	C(56)	503(6)	2042(5)	4491(4)	107(6)
C(16)	-1084(8)	2409(6)	1804(7)	128(8)	C(57)	184(8)	1536(7)	4541(6)	156(9)
C(17)	-553(7)	2648(7)	1641(6)	139(8)	C(58)	-127(7)	1288(6)	4125(7)	133(8)
C(18)	-244(6)	3097(5)	1897(4)	98(5)	C(59)	-121(5)	1528(5)	3660(5)	89(5)
C(19)	964(4)	5076(3)	4065(3)	43(3)	C(60)	188(5)	2038(4)	3611(4)	64(4)
C(20)	917(5)	5616(4)	3930(4)	66(4)	C(61)	1803(4)	2748(3)	3878(3)	46(3)
C(21)	1239(5)	6028(4)	4239(5)	81(5)	C(62)	2202(4)	3045(4)	3575(3)	56(3)
C(22)	1596(5)	5886(6)	4682(4)	82(5)	C(63)	2870(5)	2906(4)	3551(4)	76(4)
C(23)	1649(5)	5347(6)	4819(4)	82(5)	C(64)	3127(5)	2478(5)	3826(5)	80(5)
C(24)	1349(4)	4936(4)	4512(3)	65(4)	C(65)	2750(5)	2182(5)	4125(4)	81(5)
C(25)	-799(4)	3772(3)	3754(3)	45(3)	C(66)	2077(5)	2310(4)	4160(4)	71(4)
C(26)	-941(4)	3205(4)	3789(3)	56(3)	C(67)	7468(28)	2808(25)	0(18)	309(32)
C(27)	-1577(5)	3019(4)	3828(4)	77(4)	C(68)	7416(35)	5313(21)	342(18)	473(30)
C(28)	-2094(5)	3390(4)	3843(4)	78(4)	C(69)	8481(18)	2775(17)	211(14)	331(19)
C(29)	-1960(4)	3955(4)	3809(3)	62(4)	C(70)	8362(22)	4993(20)	0(18)	454(24)
C(30)	-1331(4)	4147(4)	3758(3)	53(3)	C(71)	8167(26)	3297(20)	331(18)	490(29)
C(31)	2210(4)	4250(3)	2140(3)	42(3)	C(72)	8053(28)	5603(22)	234(22)	475(30)

<sup>a</sup> Equivalent isotropic  $U$  defined as one-third of the trace of the orthogonalized  $U_{ij}$  tensor.

in CH<sub>2</sub>Cl<sub>2</sub> (40 cm<sup>3</sup>) was added [NBu<sub>4</sub>][BH<sub>4</sub>]. After 5 min the red solution was filtered through Celite, the solvent volume was reduced to ca. 5 cm<sup>3</sup> *in vacuo*, and the residue was placed on an alumina-*n*-hexane column. Elution with CH<sub>2</sub>Cl<sub>2</sub>-*n*-hexane (2:3) gave a red solution. The solvent volume was reduced *in vacuo*; further addition of *n*-hexane gave the product as a red powder, yield 0.27 g (74%). IR (CH<sub>2</sub>Cl<sub>2</sub>): 1999 and 1986 cm<sup>-1</sup>. Anal. Calcd for C<sub>66</sub>H<sub>56</sub>N<sub>4</sub>O<sub>8</sub>P<sub>2</sub>Rh<sub>2</sub>: C, 60.9; H, 4.3; N, 4.3. Found: C, 60.9; H, 4.6; N, 4.1.

[Rh<sub>2</sub>( $\mu$ -dimen)<sub>2</sub>( $\mu$ -dppm)<sub>2</sub>][PF<sub>6</sub>]<sub>2</sub> (6). A solution of dimen (0.034 g, 0.18 mmol) in methanol (2.0 cm<sup>3</sup>) was added dropwise to a slurry of [Rh<sub>2</sub>Cl<sub>2</sub>(CO)<sub>2</sub>(dppm)<sub>2</sub>]<sup>13</sup> (0.100 g, 0.091 mmol) in methanol (3.0 cm<sup>3</sup>). After all of the solid had dissolved, the resulting red solution was stirred under a vigorous nitrogen purge for 1 h. During this time the solution turned from red to purple. A solution of NH<sub>4</sub>PF<sub>6</sub> (0.036 g, 0.22 mmol) in methanol (2.0 cm<sup>3</sup>) was then added, and a lavender solid precipitated. The solid/solution mixture was stirred and cooled in an ice bath. The solid was filtered out, washed with ether, and air-dried, yield 0.131 g. The compound was purified by recrystallization from acetone/ether, yield 0.115 g (78%). Spectroscopic measurements have been reported previously.<sup>12b,e</sup>

[Rh<sub>2</sub>( $\mu$ -TM4)<sub>2</sub>( $\mu$ -dppm)<sub>2</sub>][PF<sub>6</sub>]<sub>2</sub> (7). This compound was prepared by the same method used for 6; 0.156 g (0.142 mmol) of [Rh<sub>2</sub>Cl<sub>2</sub>(CO)<sub>2</sub>(dppm)<sub>2</sub>] yielded 0.169 g (72%) of the product as the acetone solvate. The acetone of crystallization was removed *in vacuo* at room temperature. IR (Nujol mull): 2140 cm<sup>-1</sup>. <sup>31</sup>P NMR (acetone): 25.3 ppm (doublet). Anal. Calcd for C<sub>70</sub>H<sub>76</sub>N<sub>4</sub>P<sub>6</sub>F<sub>12</sub>Rh<sub>2</sub>: C, 52.8; H, 4.8; N, 3.5. Found: C, 52.9; H, 5.0; N, 3.4.

[Rh<sub>2</sub>( $\mu$ -CNCH<sub>2</sub>CH<sub>2</sub>CN)( $\mu$ -dppm)<sub>2</sub>][PF<sub>6</sub>]<sub>2</sub> (8). This compound was prepared by the same method used for 6; 0.193 g (0.176 mmol) of [Rh<sub>2</sub>

Cl<sub>2</sub>(CO)<sub>2</sub>(dppm)<sub>2</sub>] yielded 0.056 g (22%). The poor yield is due to the high solubility of the [PF<sub>6</sub>]<sup>-</sup> salt in methanol. IR (Nujol mull): 2159 cm<sup>-1</sup>. <sup>31</sup>P NMR (acetone): 27.3 ppm (doublet). Anal. Calcd for C<sub>66</sub>H<sub>56</sub>N<sub>4</sub>P<sub>6</sub>F<sub>12</sub>Rh<sub>2</sub>: C, 49.6; H, 3.9; N, 3.9. Found: C, 49.6; H, 3.8; N, 4.1.

[Rh<sub>2</sub>(CO)<sub>2</sub>(PMe<sub>2</sub>Ph)<sub>2</sub>( $\mu$ -chp)<sub>2</sub>] (10). CO gas was bubbled through a solution of [Rh<sub>2</sub>(chp)<sub>2</sub>(NBD)<sub>2</sub>] (12)<sup>12c</sup> (0.201 g, 0.031 mmol) in benzene (100 cm<sup>3</sup>); the solution turned from orange to red, whereupon PMe<sub>2</sub>Ph<sub>2</sub> (0.088 cm<sup>3</sup>, 0.062 mmol) was added and the mixture stirred for 10 min. The solution volume was reduced and precipitation induced with *n*-heptane. The orange solid was collected by filtration and the precipitation process repeated several times to obtain a total yield of 0.178 g (72%). <sup>1</sup>H NMR (toluene-*d*<sub>8</sub> solution):  $\delta$  7.972 (t, 2H, chp), 7.177 (m, 3H, Ph), 6.528 (t, 1H, chp), 6.261 (s, 1H, Ph), 6.126 (s, 1H, Ph), 1.626 (d, 6H, Me). <sup>31</sup>P NMR (toluene solution):  $\delta$  16.038 (d,  $J = 167.7$  Hz). IR (CH<sub>2</sub>Cl<sub>2</sub>/TBAH solution): 1950, 2032 cm<sup>-1</sup>. UV-visible (CH<sub>2</sub>Cl<sub>2</sub> solution):  $\lambda_{\text{max}} = 310$  nm ( $\epsilon = 1.59 \times 10^4$  M<sup>-1</sup> cm<sup>-1</sup>), 466 nm ( $\epsilon = 6.07 \times 10^3$  M<sup>-1</sup> cm<sup>-1</sup>). Anal. Calcd for C<sub>28</sub>H<sub>28</sub>Cl<sub>2</sub>N<sub>2</sub>O<sub>4</sub>Rh<sub>2</sub>: C, 42.3; H, 3.6; N, 3.5; P, 7.8. Found: C, 42.3; H, 3.7; N, 3.6; P, 7.9.

[Rh<sub>2</sub>( $\mu$ -mhp)<sub>2</sub>(NBD)<sub>2</sub>] (13). This compound was prepared by the same method used for 12, in 50% yield after recrystallization. <sup>1</sup>H NMR (CDCl<sub>3</sub>):  $\delta$  6.86 (t, 1H, mhp), 5.96 (t, 2H, mhp), 4.76 (s, 1H, nbd), 4.64 (s, 1H, nbd), 4.25 (s, 1H, nbd), 3.99 (s, 1H, nbd), 3.77 (s, 1H, nbd), 3.12 (s, 1H, nbd), 3.06 (s, 3H, mhp), 1.35 (q, 1H, nbd). Anal. Calcd for C<sub>26</sub>H<sub>28</sub>N<sub>2</sub>O<sub>2</sub>Rh<sub>2</sub>: C, 51.5; H, 4.7; N, 4.6. Found: C, 51.4; H, 4.5; N, 4.8.

**X-ray Structure Determinations of 1-C<sub>6</sub>H<sub>14</sub>, 1<sup>+</sup>[PF<sub>6</sub>]<sup>-</sup>·2C<sub>6</sub>H<sub>14</sub>, 2, 2<sup>+</sup>[PF<sub>6</sub>]<sup>-</sup>, 3-Et<sub>2</sub>O, and 3<sup>+</sup>[PF<sub>6</sub>]<sup>-</sup>·CH<sub>2</sub>Cl<sub>2</sub>.** Many of the details of the structure analyses carried out on 1-C<sub>6</sub>H<sub>14</sub>, 1<sup>+</sup>[PF<sub>6</sub>]<sup>-</sup>·2C<sub>6</sub>H<sub>14</sub>, 2, 2<sup>+</sup>[PF<sub>6</sub>]<sup>-</sup>, 3-Et<sub>2</sub>O, and 3<sup>+</sup>[PF<sub>6</sub>]<sup>-</sup>·CH<sub>2</sub>Cl<sub>2</sub> are listed in Table 1. X-ray diffraction measurements were made using Siemens four-circle P3m diffractometers

**Table 3.** Atomic Coordinates ( $\times 10^4$ ) and Equivalent Isotropic Displacement Parameters ( $\text{\AA}^2 \times 10^3$ ) for  $[\text{Rh}_2(\text{COO})_2(\text{PPh}_3)_2]_2(\mu\text{-PhNC(Me)NPh})_2[\text{PF}_6]_2 \cdot 2\text{C}_6\text{H}_{14}$  ( $1^+ \cdot [\text{PF}_6]^- \cdot 2\text{C}_6\text{H}_{14}$ )

	x	y	z	$U(\text{eq})^a$		x	y	z	$U(\text{eq})^a$
Rh(1)	636(1)	8278(1)	2892(1)	36(1)	C(34)	1140(4)	5019(3)	2397(5)	88(4)
P(1)	1183(1)	7592(1)	2269(1)	45(1)	C(33)	1678(4)	5380(4)	2610(5)	108(4)
O(1)	766(2)	6994(2)	3947(2)	77(2)	C(32)	1706(3)	6154(3)	2576(5)	88(3)
C(1)	701(2)	7465(3)	3529(3)	47(2)	N(2)	-346(2)	8937(2)	1388(2)	41(1)
C(43)	1042(2)	7785(3)	1273(3)	54(2)	N(1)	601(2)	9260(2)	2262(2)	39(1)
C(44)	1179(3)	8494(3)	1060(3)	64(2)	C(3)	151(2)	9376(2)	1596(3)	42(2)
C(45)	1080(3)	8643(4)	299(4)	78(3)	C(5)	208(3)	9977(3)	1065(3)	56(2)
C(46)	838(4)	8113(5)	-248(4)	90(3)	C(13)	-762(2)	8931(3)	618(3)	48(2)
C(47)	695(4)	7417(4)	-40(4)	92(3)	C(18)	-606(3)	8540(3)	72(3)	60(2)
C(48)	799(3)	7242(3)	709(3)	71(3)	C(17)	-1005(3)	8519(4)	-668(3)	74(3)
C(37)	2010(2)	7796(3)	2754(3)	57(2)	C(16)	-1564(4)	8876(5)	-879(4)	91(3)
C(38)	2423(3)	7847(3)	2358(4)	73(3)	C(15)	-1727(3)	9258(5)	-344(5)	99(3)
C(39)	3045(3)	8020(4)	2748(6)	97(4)	C(14)	-1331(3)	9287(4)	409(4)	72(2)
C(40)	3256(3)	8134(4)	3507(7)	107(4)	C(7)	1045(2)	9827(3)	2579(3)	43(2)
C(41)	2856(3)	8073(4)	3909(5)	94(3)	C(8)	878(3)	10558(3)	2657(3)	58(2)
C(42)	2232(3)	7905(3)	3530(4)	75(3)	C(9)	1325(3)	11104(3)	2986(4)	74(3)
C(31)	1173(2)	6570(3)	2334(3)	51(2)	C(10)	1941(3)	10921(4)	3249(4)	80(3)
C(36)	617(3)	6188(3)	2129(4)	77(3)	C(11)	2118(3)	10197(4)	3193(4)	80(3)
C(35)	605(3)	5413(3)	2156(4)	86(3)	C(12)	1674(2)	9657(3)	2860(3)	61(2)
C(49)	2383(10)	2806(11)	4723(10)	257(9)	P(2)	0	2972(1)	2500	65(1)
C(50)	869(10)	4864(12)	13(12)	272(9)	F(1)	688(2)	2948(3)	3064(3)	133(2)
C(51)	2172(11)	3651(14)	4506(11)	267(9)	F(2)	-22(6)	2160(5)	2816(7)	124(8)
C(52)	1332(15)	4947(18)	4651(16)	343(13)	F(3)	-272(7)	3277(9)	3095(7)	147(8)
C(53)	224(16)	4919(23)	4985(23)	213(13)	F(4)	6(7)	3743(5)	2162(8)	146(10)
C(54)	1725(15)	4340(20)	4587(16)	346(13)	F(5)	234(7)	2589(10)	1899(7)	155(9)

<sup>a</sup> Equivalent isotropic  $U$  defined as one-third of the trace of the orthogonalized  $U_{ij}$  tensor.

**Table 4.** Atomic Coordinates ( $\times 10^4$ ) and Equivalent Isotropic Displacement Parameters ( $\text{\AA}^2 \times 10^3$ ) for  $[\text{Rh}_2(\text{CO})_2\{\text{P(OPh)}_3\}_2(\mu\text{-PhNC(Me)NPh})_2\} (2)$ 

	x	y	z	$U(\text{eq})^a$		x	y	z	$U(\text{eq})^a$
Rh(1)	9708(1)	2385(1)	6612(1)	34(1)	C(17)	8529(3)	3062(3)	10233(4)	95(3)
P(1)	8894(1)	1687(1)	6686(1)	36(1)	C(18)	8691(2)	3045(2)	9416(3)	67(2)
O(1)	10308(1)	1155(2)	5822(2)	66(1)	C(31)	7929(2)	1589(2)	7523(2)	43(1)
O(3)	8411(1)	2008(1)	7257(2)	46(1)	C(32)	8050(2)	1268(2)	8321(3)	54(1)
O(4)	8404(1)	1494(1)	5810(2)	45(1)	C(33)	7576(2)	853(3)	8584(3)	63(2)
O(5)	9046(1)	885(1)	7106(2)	46(1)	C(34)	7000(2)	765(3)	8060(3)	67(2)
N(1)	9278(1)	3315(2)	7062(2)	38(1)	C(35)	6886(2)	1094(3)	7269(3)	66(2)
N(2)	9511(1)	3068(2)	8512(2)	40(1)	C(36)	7353(2)	1519(2)	6991(3)	56(2)
C(1)	10072(2)	1622(2)	6125(2)	44(1)	C(37)	8587(2)	1457(2)	4996(2)	45(1)
C(3)	9212(2)	3470(2)	7857(2)	41(1)	C(38)	8673(2)	786(3)	4650(3)	65(2)
C(5)	8831(2)	4135(2)	8017(3)	55(1)	C(39)	8833(3)	749(3)	3845(3)	82(2)
C(7)	9005(2)	3795(2)	6376(2)	40(1)	C(40)	8909(3)	1377(3)	3399(3)	79(2)
C(8)	9348(2)	4357(2)	6105(3)	54(1)	C(41)	8819(3)	2045(3)	3750(3)	78(2)
C(9)	9086(2)	4815(3)	5435(3)	66(2)	C(42)	8658(2)	2095(3)	4565(3)	62(2)
C(10)	8472(2)	4705(3)	5025(3)	64(2)	C(43)	8899(2)	203(2)	6712(2)	45(1)
C(11)	8121(2)	4152(3)	5280(3)	62(2)	C(44)	8285(2)	-58(2)	6584(3)	56(1)
C(12)	8383(2)	3694(2)	5958(3)	52(1)	C(45)	8158(3)	-729(3)	6190(3)	79(2)
C(13)	9322(2)	3096(2)	9327(2)	52(1)	C(46)	8635(4)	-1129(3)	5946(3)	94(3)
C(14)	9779(3)	3142(3)	10060(3)	72(2)	C(47)	9245(3)	-881(3)	6105(3)	83(2)
C(15)	9608(4)	3142(3)	10865(3)	100(3)	C(48)	9381(2)	-202(2)	6494(3)	62(2)
C(16)	8992(4)	3108(3)	10953(4)	109(3)					

<sup>a</sup> Equivalent isotropic  $U$  defined as one-third of the trace of the orthogonalized  $U_{ij}$  tensor.

on single crystals mounted in thin-walled glass capillaries. Graphite-monochromatized molybdenum  $K\alpha$  radiation ( $\lambda = 0.71073 \text{ \AA}$ ) was used as the X-ray source. Cell dimensions for each analysis were determined from 25 centered reflections, and the reciprocal lattice symmetry and cell axis lengths were checked by partial rotation photographs about the unit cell axes.

For each structure analysis intensity data were collected for unique quadrants of reciprocal space, for  $4 \leq 2\theta \leq 50^\circ$  at variable scan speeds, those speeds being based on a prescan. Those reflections for  $2\theta > 40^\circ$  with a prescan count below a low threshold were either excluded or collected at maximum scan speed. Corrections were applied for Lorentz and polarization effects, long-term intensity fluctuations (on the basis of the intensities of three check reflections repeatedly measured during data collection), and X-ray absorption (on the basis of azimuthal scan data). The structures were solved by heavy-atom (Patterson and difference Fourier) methods and refined by least-squares against  $F$  using only those reflections for which  $I > 3\sigma(I)$ . Reflections were weighted according to the formula  $w^{-1} = \sigma_o^2(F_o) + gF_o^2$ , where  $\sigma_o^2(F_o)$  is the variance in  $F_o$  arising from counting statistics and  $g$  (see Table 1) was chosen to give

minimum variation in the average values of  $S$  as a function of  $F_o$ .

$$R = \sum |\Delta| / \sum |F_o|; R_w = [ \sum w^{1/2} |\Delta| / \sum w^{1/2} |F_o| ];$$

$$S = [ \sum w \Delta^2 / (N_{\text{obs}} - N_{\text{var}}) ]^{1/2}; \Delta = F_o - F_c$$

The hexane solvent molecules of  $1 \cdot \text{C}_6\text{H}_{14}$  and  $1^+ \cdot \text{PF}_6^- \cdot 2\text{C}_6\text{H}_{14}$  showed severe disorder, and the electron density was modeled by carbon positions which gave unsatisfactory molecular geometry. The  $[\text{PF}_6]^-$  anion of  $1^+ \cdot \text{PF}_6^- \cdot 2\text{C}_6\text{H}_{14}$  showed a 2-fold site disorder [atoms F(2-5) having 50% occupancy] and was subject to geometry restraints (P-F, F...F distances). In  $1^+ \cdot \text{PF}_6^- \cdot 2\text{C}_6\text{H}_{14}$  and 2 the dirhodium species (and the  $[\text{PF}_6]^-$  anion) lie at sites of crystallographic 2-fold rotational symmetry. All hydrogen atoms were constrained to ideal geometries (with C-H = 0.96 \text{ \AA}) and were assigned fixed isotropic displacement parameters.

Final difference syntheses showed no chemically significant features, the largest maxima being close to the metal, solvent, or anion atoms. Refinements converged (mean shift/esd  $\ll 0.1$ ) smoothly to the residuals given in Table 1. Tables 2-7 report the positional parameters for these structure determinations. Full tables of interatomic distances and bond

**Table 5.** Atomic Coordinates ( $\times 10^4$ ) and Equivalent Isotropic Displacement Parameters ( $\text{\AA}^2 \times 10^3$ ) for [Rh<sub>2</sub>(CO)<sub>2</sub>]P(OPh)<sub>3</sub>]<sub>2</sub>[ $\mu$ -PhNC(Me)NPh]<sub>2</sub>][PF<sub>6</sub>]<sub>2</sub> ( $2^+$ ·[PF<sub>6</sub>]<sup>-</sup>)

	x	y	z	U(eq) <sup>a</sup>		x	y	z	U(eq) <sup>a</sup>
Rh(2)	2842(1)	2072(1)	1020(1)	16(1)	C(30)	3986(4)	477(2)	1078(2)	37(1)
Rh(1)	4472(1)	2982(1)	1186(1)	16(1)	C(37)	4744(4)	4624(2)	1560(2)	29(1)
P(1)	3724(1)	3580(1)	1743(1)	20(1)	C(42)	5825(4)	4580(2)	1455(2)	44(2)
P(2)	2079(1)	2341(1)	209(1)	20(1)	C(41)	6080(5)	4946(3)	1054(3)	63(2)
N(1)	5181(2)	2345(2)	1768(1)	19(1)	C(40)	5290(6)	5346(3)	773(2)	69(2)
N(2)	3543(3)	1777(1)	1773(1)	19(1)	C(39)	4229(6)	5403(2)	896(2)	59(2)
N(3)	5275(3)	2434(1)	689(1)	20(1)	C(38)	3938(4)	5038(2)	1294(2)	44(2)
N(4)	4120(3)	1571(1)	759(1)	20(1)	C(31)	3644(4)	3423(2)	2783(1)	29(1)
O(1)	3615(2)	3920(1)	331(1)	32(1)	C(32)	2705(4)	3287(2)	2987(2)	36(1)
O(2)	873(2)	2646(2)	1427(1)	37(1)	C(33)	2746(5)	3411(3)	3516(2)	47(2)
O(4)	4435(2)	4219(1)	1948(1)	25(1)	C(34)	3725(5)	3672(3)	3810(2)	54(2)
O(3)	3611(3)	3238(1)	2263(1)	32(1)	C(35)	4656(5)	3816(3)	3592(2)	53(2)
O(5)	2475(2)	3835(1)	1481(1)	29(1)	C(36)	4626(4)	3689(2)	3068(2)	39(2)
O(6)	1378(2)	3001(1)	181(1)	28(1)	C(43)	1670(3)	4167(2)	1714(2)	28(1)
O(7)	2975(2)	2417(1)	-154(1)	28(1)	C(44)	1959(4)	4531(2)	2154(2)	33(1)
O(8)	1192(2)	1829(1)	-106(1)	24(1)	C(45)	1073(4)	4830(2)	2350(2)	41(2)
C(1)	3930(3)	3570(2)	654(1)	22(1)	C(46)	-54(4)	4770(2)	2101(2)	48(2)
C(2)	1620(3)	2448(2)	1269(1)	23(1)	C(47)	-307(4)	4409(2)	1653(2)	44(2)
C(3)	4627(3)	1906(2)	1988(1)	19(1)	C(48)	548(3)	4108(2)	1451(2)	35(1)
C(4)	5015(3)	1822(2)	599(1)	22(1)	C(49)	754(3)	3342(2)	-245(2)	29(1)
C(5)	5234(3)	1555(2)	2464(2)	28(1)	C(50)	751(4)	3999(2)	-188(2)	40(2)
C(6)	5772(3)	1378(2)	358(2)	27(1)	C(51)	141(5)	4370(3)	-586(2)	54(2)
C(7)	6399(3)	2428(2)	1898(1)	19(1)	C(52)	-449(5)	4082(3)	-1028(2)	55(2)
C(8)	7136(3)	1956(2)	1791(1)	27(1)	C(53)	-447(4)	3422(3)	-1081(2)	48(2)
C(9)	8314(4)	2073(2)	1890(2)	35(1)	C(54)	161(4)	3042(2)	-685(2)	36(1)
C(10)	8741(3)	2655(3)	2082(2)	36(1)	C(55)	2847(3)	2540(2)	-694(1)	25(1)
C(11)	8005(3)	3133(2)	2188(2)	30(1)	C(56)	2985(4)	3160(2)	-848(2)	35(1)
C(12)	6832(3)	3013(2)	2102(1)	22(1)	C(57)	2957(4)	3277(2)	-1370(2)	40(2)
C(13)	2759(3)	1480(2)	2047(2)	24(1)	C(58)	2821(4)	2772(2)	-1717(2)	38(1)
C(14)	1993(3)	1024(2)	1791(2)	31(1)	C(59)	2670(5)	2153(2)	-1545(2)	50(2)
C(15)	1135(4)	776(2)	2026(2)	39(2)	C(60)	2688(4)	2028(2)	-1029(2)	40(2)
C(16)	1041(4)	967(3)	2517(2)	42(2)	C(61)	410(3)	1542(2)	175(1)	25(1)
C(17)	1806(4)	1411(3)	2774(2)	42(2)	C(62)	535(4)	904(2)	297(2)	40(2)
C(18)	2654(3)	1671(2)	2541(2)	31(1)	C(63)	-206(4)	630(2)	588(2)	48(2)
C(19)	6064(3)	2757(2)	430(2)	23(1)	C(64)	-1030(4)	1005(3)	757(2)	45(2)
C(20)	6938(3)	3126(2)	711(2)	30(1)	C(65)	-1138(3)	1637(2)	621(2)	39(2)
C(21)	7702(4)	3443(2)	456(2)	37(1)	C(66)	-432(3)	1921(2)	322(2)	33(1)
C(22)	7619(4)	3382(2)	-72(2)	37(2)	P(3)	7401(1)	-113(1)	1822(1)	40(1)
C(23)	6749(4)	3016(2)	-352(2)	38(2)	F(1)	7063(4)	316(2)	2263(2)	95(2)
C(24)	5962(4)	2714(2)	-108(2)	31(1)	F(2)	7740(4)	-542(2)	1382(2)	105(2)
C(25)	3838(3)	903(2)	668(2)	25(1)	F(3)	8561(3)	257(2)	1879(1)	79(1)
C(26)	3396(3)	688(2)	171(2)	33(1)	F(4)	7974(3)	-625(2)	2245(1)	74(1)
C(27)	3104(4)	44(2)	86(2)	45(2)	F(5)	6846(3)	395(2)	1392(1)	67(1)
C(28)	3224(4)	-373(2)	496(2)	49(2)	F(6)	6232(3)	-482(2)	1776(2)	107(2)
C(29)	3679(5)	-161(2)	992(2)	51(2)					

<sup>a</sup> Equivalent isotropic  $U$  defined as one-third of the trace of the orthogonalized  $U_{ij}$  tensor.

angles, displacement parameters, and hydrogen atomic parameters are given in the supplementary material.

All structure analysis calculations were made<sup>16</sup> with programs written by G. M. Sheldrick as implemented on Siemens structure determination systems. Complex neutral-atom scattering factors were taken from ref 17.

## Results and Discussion

The X-ray structure analyses of **1**·C<sub>6</sub>H<sub>14</sub>, **1**<sup>+</sup>·PF<sub>6</sub><sup>-</sup>·2C<sub>6</sub>H<sub>14</sub>, **2**, **2**<sup>+</sup>·PF<sub>6</sub><sup>-</sup>, **3**·Et<sub>2</sub>O, and **3**<sup>+</sup>·PF<sub>6</sub><sup>-</sup>·CH<sub>2</sub>Cl<sub>2</sub> were carried out in order to observe the changes in molecular geometry for the pairs of dirhodium complexes in different oxidation states. The molecular geometries of **1**<sup>+</sup>, **2**<sup>+</sup>, and **3**<sup>+</sup> are illustrated in Figures 1–3; the cations have gross geometries essentially rather close to their corresponding neutral species. A brief summary of the most important molecular parameters is given in Table 8 for the species **1**, **1**<sup>+</sup>, **2**, **2**<sup>+</sup>, **3**, and **3**<sup>+</sup> as well as for **4** and **4**<sup>+</sup><sup>11c</sup> for comparison. In all of the complexes the bridging acetamidinate ligands are mutually *cis* and the rhodium coordination environment is approximately square planar (two *cis* nitrogen donors *trans* to CO and a phosphorus ligand). The gross molecular geometry is

therefore opened out from the classic face-to-face structure observed for [Rh<sub>2</sub>( $\mu$ -carboxylate)<sub>4</sub>] species in which the RhO<sub>4</sub> planes are parallel. For the acetamidinate complexes the second rhodium atom lies above the coordination plane at Rh...Rh distances between 2.685(1) and 2.991(2) Å. The complexes show approximate C<sub>2</sub> symmetry in 6 of the 8 cases [the other two, **1**<sup>+</sup> and **2**, having *exact* crystallographic C<sub>2</sub> symmetry]. The coordination planes of the two rhodium atoms are inclined to one another by varying amounts and further exhibit a torsion about the Rh...Rh vector (*cf.* P–Rh...Rh–C and N–Rh...Rh–N torsion angles  $\gg$  0°) in a sense which moves the bulky phosphorus ligands further apart. The rhodium atoms all lie slightly out of the coordination planes *toward* the second rhodium. The replacement of PPh<sub>3</sub> by P(OPh)<sub>3</sub> apparently allows the rhodium atoms to approach one another more closely. Thus, the Rh...Rh distances fall with increasing substitution of PPh<sub>3</sub> by P(OPh)<sub>3</sub> across the series **1** > **3** > **2** and **1**<sup>+</sup> > **3**<sup>+</sup> > **2**<sup>+</sup>. Increased delocalization of Rh d<sub>z</sub> electron density on to the phosphorus ligand may play a role here by reducing Rh  $\pi$  and  $\delta$  antibonding interactions. The reasons for this are presumably related to the greater flexibility of P(OPh)<sub>3</sub> and hence reduced steric interference between the ligands on different rhodium atoms. Consistent with the latter suggestion, we note the decrease of average ligand–Rh...Rh–ligand torsion angles (2 $\gamma$ ) about the Rh...Rh vector across these series (see

(16) Sheldrick, G. M. SHELXTL, Göttingen, FRG, 1985, 1990.

(17) *International Tables for X-ray Crystallography*; Kynoch Press: Birmingham, U.K., 1974; Vol. IV.

**Table 6.** Atomic Coordinates ( $\times 10^4$ ) and Equivalent Isotropic Displacement Parameters ( $\text{\AA}^2 \times 10^3$ ) for  $[\text{Rh}_2(\text{CO})_2(\text{PPh}_3)\{\text{P}(\text{OPh})_3\}\mu\text{-PhNC}(\text{Me})\text{NPh}]_2 \cdot \text{Et}_2\text{O}$  (**3**·Et<sub>2</sub>O)

	<i>x</i>	<i>y</i>	<i>z</i>	<i>U</i> (eq) <sup>a</sup>		<i>x</i>	<i>y</i>	<i>z</i>	<i>U</i> (eq) <sup>a</sup>
Rh(1)	4595(1)	2554(1)	788(1)	35(1)	C(30)	1087(3)	1870(2)	1677(2)	61(1)
Rh(2)	3872(1)	1413(1)	988(1)	35(1)	C(31)	6624(2)	2231(2)	-167(2)	48(1)
P(1)	5368(1)	2555(1)	-182(1)	41(1)	C(32)	7363(3)	2426(2)	-567(2)	68(1)
P(2)	4860(1)	1121(1)	1810(1)	39(1)	C(33)	8281(3)	2150(2)	-560(2)	82(2)
N(3)	3912(2)	2663(1)	1704(1)	39(1)	C(34)	8473(3)	1689(2)	-155(2)	83(2)
N(4)	2933(2)	1854(1)	1634(1)	39(1)	C(35)	7749(3)	1495(2)	248(2)	73(2)
N(1)	3136(2)	2623(1)	336(1)	39(1)	C(36)	6830(3)	1766(2)	247(2)	57(1)
N(2)	2826(2)	1661(1)	225(1)	41(1)	C(37)	5608(2)	3283(1)	-480(2)	47(1)
O(1)	6542(2)	2579(1)	1556(1)	73(1)	C(38)	5653(3)	3425(2)	-1145(2)	63(1)
O(2)	5060(2)	733(1)	75(1)	75(1)	C(39)	5842(3)	3977(2)	-1336(2)	86(2)
O(3)	4975(2)	1530(1)	2444(1)	50(1)	C(40)	5966(3)	4403(2)	-869(3)	93(2)
O(4)	4697(2)	522(1)	2180(1)	53(1)	C(41)	5922(3)	4276(2)	-210(2)	79(2)
O(5)	6013(2)	1057(1)	1621(1)	54(1)	C(42)	5740(3)	3717(2)	-16(2)	59(1)
C(1)	5806(2)	2564(1)	1240(2)	45(1)	C(43)	4733(3)	2222(2)	-914(2)	53(1)
C(2)	4609(3)	998(1)	423(1)	46(1)	C(44)	5135(4)	1755(2)	-1226(2)	78(2)
C(3)	2548(2)	2195(1)	112(1)	42(1)	C(45)	4642(5)	1515(2)	-1778(2)	103(2)
C(4)	3170(2)	2355(1)	1924(1)	39(1)	C(46)	3758(5)	1728(3)	-2018(2)	103(2)
C(5)	1598(3)	2323(2)	-296(2)	58(1)	C(47)	3335(4)	2192(2)	-1717(2)	85(2)
C(6)	2614(3)	2564(2)	2507(2)	59(1)	C(48)	3822(3)	2435(2)	-1164(2)	64(1)
C(7)	2726(2)	3185(1)	382(2)	44(1)	C(49)	4775(3)	1409(1)	3097(1)	44(1)
C(8)	1946(3)	3300(2)	789(2)	54(1)	C(50)	5545(3)	1438(2)	3561(2)	60(1)
C(9)	1597(3)	3852(2)	867(2)	65(1)	C(51)	5364(4)	1346(2)	4216(2)	75(2)
C(10)	2031(3)	4295(2)	552(2)	75(2)	C(52)	4435(4)	1220(2)	4401(2)	79(2)
C(11)	2802(3)	4189(2)	142(2)	68(1)	C(53)	3653(3)	1196(2)	3929(2)	78(2)
C(12)	3147(3)	3642(1)	58(2)	55(1)	C(54)	3818(3)	1292(2)	3273(2)	63(1)
C(13)	2282(3)	1201(1)	-86(2)	50(1)	C(55)	4033(2)	82(1)	2014(2)	46(1)
C(14)	1332(3)	1059(2)	118(2)	79(2)	C(56)	3522(3)	-147(2)	2515(2)	65(1)
C(15)	823(4)	592(2)	-165(3)	107(2)	C(57)	2846(3)	-580(2)	2374(3)	88(2)
C(16)	1284(6)	269(2)	-631(3)	121(3)	C(58)	2684(4)	-778(2)	1748(3)	91(2)
C(17)	2145(5)	421(3)	-855(3)	118(3)	C(59)	3207(4)	-554(2)	1252(2)	86(2)
C(18)	2649(3)	905(2)	-586(2)	92(2)	C(60)	3911(3)	-127(1)	1381(2)	65(1)
C(19)	4325(2)	3132(1)	2081(1)	43(1)	C(61)	6787(3)	911(2)	2086(2)	59(1)
C(20)	4280(3)	3678(1)	1817(2)	53(1)	C(62)	7396(3)	1334(2)	2340(2)	76(2)
C(21)	4728(3)	4129(2)	2147(2)	73(2)	C(63)	8171(3)	1172(3)	2797(3)	107(3)
C(22)	5239(3)	4054(2)	2746(2)	77(2)	C(64)	8324(4)	620(4)	2976(3)	118(3)
C(23)	5300(3)	3510(2)	3015(2)	81(2)	C(65)	7720(4)	210(3)	2691(3)	110(3)
C(24)	4851(3)	3053(2)	2682(2)	65(1)	C(66)	6937(3)	349(2)	2245(2)	80(2)
C(25)	1994(2)	1585(1)	1711(1)	42(1)	O(6)	3970(2)	1109(2)	6071(2)	90(1)
C(26)	1958(3)	996(1)	1768(2)	54(1)	C(67)	3462(5)	592(3)	6006(4)	137(3)
C(27)	1061(3)	703(2)	1797(2)	63(1)	C(68)	4145(5)	121(3)	6073(3)	138(3)
C(28)	184(3)	986(2)	1770(2)	68(1)	C(69)	3337(4)	1581(2)	6018(3)	92(2)
C(29)	192(3)	1574(2)	1709(2)	76(2)	C(70)	3948(4)	2093(2)	6099(3)	117(3)

<sup>a</sup> Equivalent isotropic *U* defined as one-third of the trace of the orthogonalized  $U_{ij}$  tensor.

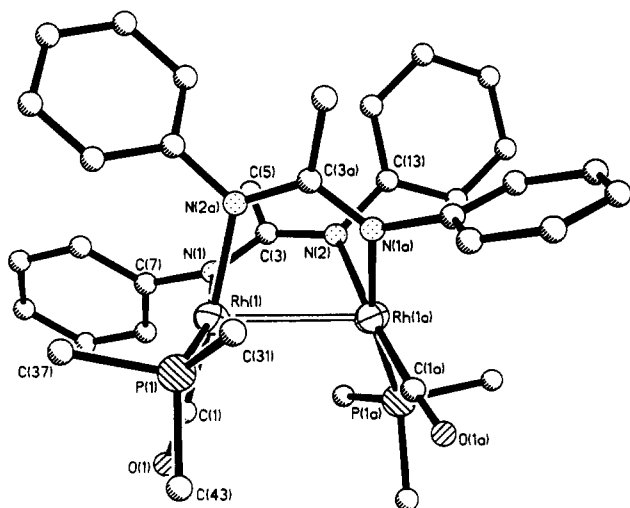


**Figure 1.** Molecular structure of **1**<sup>+</sup> showing the atom-labeling scheme. All hydrogen atoms and all but the *ipso* carbons of the phosphorus ligand have been omitted for clarity.

Table 9), with much larger effects for the first substitution (*i.e.* for **1** compared with **3**) than for the second. In addition the replacement of  $\mu\text{-RNNR}$  ( $R = p\text{-tolyl}$ ) by  $\text{PhNC}(\text{Me})\text{NPh}$  apparently keeps the rhodium atoms further apart (see Table 8) and requires slightly greater torsions about the Rh...Rh vector.

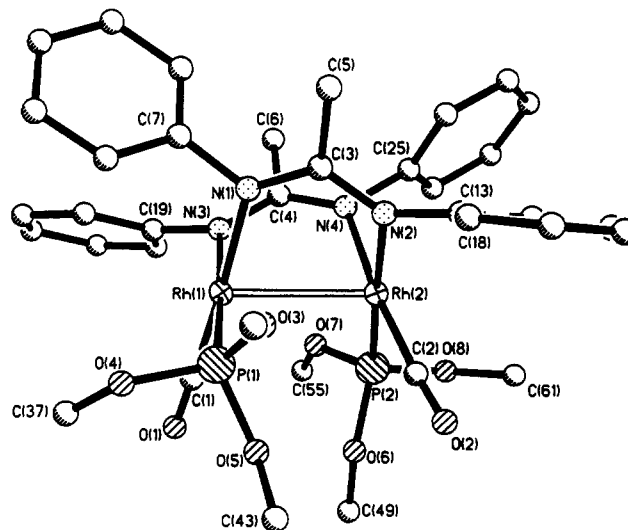


**Figure 2.** Molecular structure of **2**<sup>+</sup> showing the atom-labeling scheme. All hydrogen atoms and all but the *ipso* carbons of the phosphorus ligand have been omitted for clarity.

The most striking effect of oxidation of these complexes (*e.g.* of **1** to **1**<sup>+</sup>) is on the Rh...Rh separation. In each of the four cases the Rh...Rh distance falls substantially, by between 0.147(2) and 0.262(4) Å. In addition the angle between the two least-squares planes containing the rhodium atoms ( $2\beta$ ) and their associated

**Table 7.** Atomic Coordinates ( $\times 10^4$ ) and Equivalent Isotropic Displacement Parameters ( $\text{\AA}^2 \times 10^3$ ) for [Rh<sub>2</sub>(CO)<sub>2</sub>(PPh<sub>3</sub>)<sub>2</sub>{P(OPh)<sub>3</sub>}<sub>2</sub>{ $\mu$ -PhNC(Me)Ph]<sub>2</sub>[PF<sub>6</sub>]<sub>2</sub>·CH<sub>2</sub>Cl<sub>2</sub> (3<sup>+</sup>·[PF<sub>6</sub>]<sup>-</sup>·CH<sub>2</sub>Cl<sub>2</sub>)

	<i>x</i>	<i>y</i>	<i>z</i>	<i>U</i> (eq) <sup>a</sup>		<i>x</i>	<i>y</i>	<i>z</i>	<i>U</i> (eq) <sup>a</sup>
Rh(1)	1362(1)	549(1)	2260(1)	36(1)	C(33)	2189(4)	-1537(3)	883(3)	76(2)
Rh(2)	2760(1)	682(1)	330(1)	36(1)	C(34)	3136(4)	-1419(3)	950(3)	73(2)
P(1)	1062(1)	-386(1)	2129(1)	42(1)	C(35)	3460(4)	-990(3)	1366(3)	73(2)
P(2)	3960(1)	895(1)	2675(1)	48(1)	C(36)	2838(4)	-680(2)	1712(3)	57(2)
O(1)	2416(3)	505(2)	977(2)	68(2)	C(37)	-50(3)	-469(2)	1569(2)	47(2)
O(2)	3477(3)	-471(2)	3416(2)	68(1)	C(38)	-681(4)	-888(2)	1674(3)	60(2)
O(3)	4055(2)	444(2)	2079(2)	63(1)	C(39)	-1480(4)	-968(3)	1220(3)	72(2)
N(1)	511(3)	642(2)	3085(2)	42(1)	C(40)	-1651(4)	-614(3)	667(3)	78(3)
O(4)	5002(2)	884(2)	3043(2)	58(1)	C(41)	-1058(4)	-188(3)	564(3)	79(3)
O(5)	3893(3)	1454(2)	2247(2)	76(2)	C(42)	-244(4)	-113(2)	1014(3)	61(2)
N(2)	1698(3)	478(2)	3944(2)	42(1)	C(43)	899(4)	-811(2)	2894(3)	50(2)
N(3)	1460(3)	1401(2)	2238(2)	42(1)	C(44)	1516(4)	-1241(2)	3092(3)	66(2)
N(4)	2264(3)	1485(1)	3317(2)	43(1)	C(45)	1342(5)	-1570(3)	3653(3)	82(3)
C(1)	2043(3)	511(2)	1476(3)	46(2)	C(46)	566(6)	-1479(3)	4017(3)	93(3)
C(2)	3206(3)	-35(2)	3368(2)	45(2)	C(47)	-41(5)	-1059(3)	3838(3)	78(3)
C(3)	795(3)	556(2)	3755(2)	42(1)	C(48)	125(4)	-720(2)	3278(3)	61(2)
C(4)	1779(3)	1718(2)	2761(2)	44(2)	C(49)	4774(4)	396(2)	1633(3)	59(2)
C(5)	88(3)	535(2)	4293(3)	59(2)	C(50)	4707(5)	666(3)	1010(3)	80(3)
C(6)	1624(4)	2326(2)	2724(3)	64(2)	C(51)	5396(6)	589(4)	541(4)	106(4)
C(7)	-404(3)	872(2)	2907(2)	46(2)	C(52)	6111(6)	234(5)	716(6)	127(5)
C(8)	-660(4)	1378(2)	3157(3)	58(2)	C(53)	6154(5)	-52(4)	1338(6)	113(4)
C(9)	-1524(4)	1601(3)	2967(3)	76(2)	C(54)	5493(5)	23(3)	1808(4)	92(3)
C(10)	-2165(5)	1334(3)	2500(4)	86(3)	C(55)	5281(3)	1041(2)	3736(3)	54(2)
C(11)	-1918(4)	839(3)	2245(3)	84(3)	C(56)	5887(4)	1481(2)	3827(3)	68(2)
C(12)	-1048(4)	599(2)	2444(3)	62(2)	C(57)	6205(5)	1639(3)	4492(4)	89(3)
C(13)	2009(3)	268(2)	4625(2)	47(2)	C(58)	5910(6)	1361(4)	5062(4)	105(4)
C(14)	1985(4)	-280(2)	4761(3)	63(2)	C(59)	5330(5)	916(4)	4967(3)	92(3)
C(15)	2288(4)	-489(3)	5418(4)	79(3)	C(60)	5004(4)	746(3)	4292(3)	69(2)
C(16)	2630(5)	-144(4)	5927(4)	95(3)	C(61)	4527(4)	1896(2)	2319(3)	61(2)
C(17)	2669(6)	399(4)	5800(4)	116(4)	C(62)	5218(5)	1932(3)	1866(3)	78(3)
C(18)	2361(5)	612(3)	5148(3)	86(3)	C(63)	5849(5)	2368(3)	1946(4)	95(3)
C(19)	1101(3)	1629(2)	1581(3)	48(2)	C(64)	5775(6)	2732(3)	2470(6)	113(4)
C(20)	148(4)	1607(3)	1379(3)	75(2)	C(65)	5035(7)	2698(3)	2892(5)	116(4)
C(21)	-192(5)	1782(3)	716(4)	101(3)	C(66)	4396(5)	2272(3)	2810(4)	86(3)
C(22)	407(5)	1975(3)	263(3)	90(3)	C(67)	4193(8)	1808(7)	7318(8)	283(11)
C(23)	1343(5)	1993(3)	444(3)	85(3)	Cl(1)	4896(3)	1470(2)	6895(2)	252(3)
C(24)	1696(4)	1818(2)	1104(3)	65(2)	Cl(2)	3057(3)	1523(3)	7219(2)	299(4)
C(25)	2382(3)	1763(2)	3975(2)	44(2)	P(3)	3975(1)	2035(1)	9518(1)	84(1)
C(26)	3273(3)	1783(2)	4335(3)	54(2)	F(1)	3086(3)	2111(2)	8994(3)	151(3)
C(27)	3390(4)	2008(2)	4997(3)	64(2)	F(2)	4518(4)	2406(4)	9075(5)	265(5)
C(28)	2639(4)	2214(2)	5313(3)	67(2)	F(3)	4321(6)	1549(4)	9105(4)	233(5)
C(29)	1747(4)	2198(2)	4960(3)	67(2)	F(4)	3435(4)	1610(3)	9920(4)	177(3)
C(30)	1625(3)	1967(2)	4299(3)	56(2)	F(5)	4882(3)	1956(3)	10035(3)	163(3)
C(31)	1889(3)	-790(2)	1647(3)	48(2)	F(6)	3632(6)	2474(4)	9941(5)	284(6)
C(32)	1568(4)	-1221(2)	1220(3)	68(2)					

<sup>a</sup> Equivalent isotropic *U* defined as one-third of the trace of the orthogonalized *U*<sub>ij</sub> tensor.

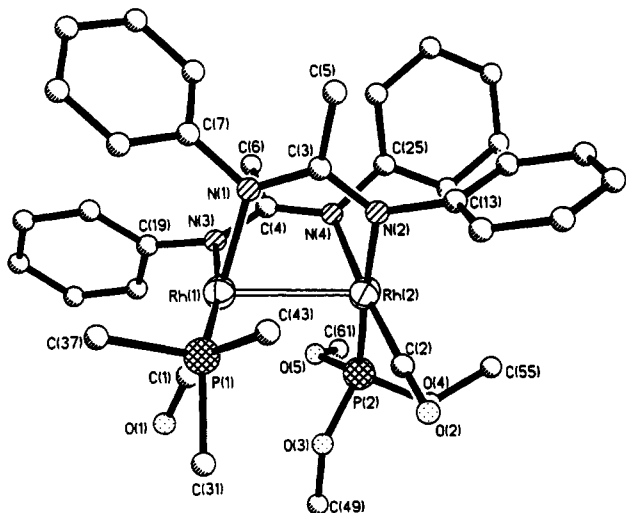


**Figure 3.** Molecular structure of 3<sup>+</sup> showing the atom-labeling scheme. All hydrogen atoms and all but the *ipso* carbons of the phosphorus ligand have been omitted for clarity.

four ligand atoms falls, in each case, by between 9.5 and 4.6° (see Table 9). The effect on the torsion about the Rh...Rh vector is

less clear-cut although in general the degree of twist ( $2\gamma$ ) is slightly reduced on oxidation.

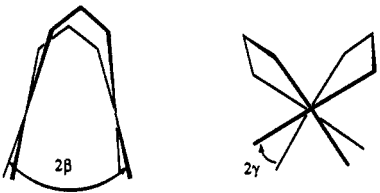
Other bond length changes on oxidation are less dramatic but understandable. Thus the Rh-P and Rh-C(O) distances uniformly increase and the Rh-N distances decrease as a result of oxidation. This is consistent with a higher effective oxidation state for the rhodium atoms and consequently lowered metal orbital energies. Thus nitrogen donor ligands seem to behave as  $\sigma$  donors which see a more strongly electron-accepting rhodium in the cationic complexes and hence form stronger shorter bonds. In contrast the CO, PPh<sub>3</sub>, and P(OPh)<sub>3</sub> ligands apparently show the effects of loss of  $\pi$ -bonding with rhodium atoms that are more electron poor in the oxidized complexes and the metal-ligand distances therefore increase. In addition the C-O and P-C (and P-O) distances and C-P-C (and O-P-O) angles show small changes in their average values consistent with established models of their  $\pi$ -acceptor orbitals (C-O  $\pi^*$  and partly P-C or P-O  $\sigma^*$ , respectively).<sup>18</sup> The N-C-N bond angles appear to be rather insensitive to the oxidation of the complex although the N-N-N angles of 4 and 4<sup>+</sup> seem more flexible. In addition the C-N-Rh (and N-N-Rh) angles show reductions on oxidation in all cases, as the Rh...Rh distance spanned by the bridging ligands is reduced.

These observations are all consistent with oxidation being in

**Table 8.** Molecular Dimensions<sup>a</sup> for Dirhodium species **1**, **1**<sup>+</sup>, **2**, **2**<sup>+</sup>, **3**, **3**<sup>+</sup>, **4**, **11**<sup>e</sup> and **4**<sup>11e</sup>

param	complex							
	1	1 <sup>+</sup>	2	2 <sup>+</sup>	3	3 <sup>+</sup>	4	4 <sup>+</sup>
Distances (Å)								
Rh...Rh	2.991(2)	2.771(1)	2.853(1)	2.685(1)	2.875(1)	2.728(1)	2.960(4)	2.698(1)
Rh...plane dist	-0.115, -0.130	-0.124	-0.049	-0.046, -0.054	-0.087, <sup>b</sup> -0.055 <sup>c</sup>	-0.103, <sup>b</sup> -0.042 <sup>c</sup>	-0.130, -0.097	-0.104, -0.092
Rh-P(av)	2.274(2)	2.336(2)	2.173(1)	2.227(1)	2.270(2), <sup>b</sup> 2.176(2) <sup>c</sup>	2.332(2), <sup>b</sup> 2.242(2) <sup>c</sup>	2.290(5)	2.335(1)
Rh-C(av)	1.809(8)	1.854(5)	1.825(4)	1.877(4)	1.816(3), <sup>b</sup> 1.831(3) <sup>c</sup>	1.862(5), <sup>b</sup> 1.861(5) <sup>c</sup>	1.814(15)	1.856(3)
C-O(av)	1.151(10)	1.123(7)	1.137(5)	1.128(5)	1.141(4)	1.134(6)	1.174(20)	1.134(5)
Rh-N(trans to C)(av)	2.132(6)	2.100(4)	2.107(3)	2.070(3)	2.116(2), <sup>b</sup> 2.129(2) <sup>c</sup>	2.089(4), <sup>b</sup> 2.083(4) <sup>c</sup>	2.137(18)	2.097(3)
Rh-N(trans to P)(av)	2.129(6)	2.068(4)	2.118(3)	2.093(3)	2.130(2), <sup>b</sup> 2.108(2) <sup>c</sup>	2.084(4), <sup>b</sup> 2.080(4) <sup>c</sup>	2.137(18)	2.096(3)
P-A (A = C, O) (av)	1.835(9)	1.825(6)	1.607(3)	1.594(3)	1.841(3), <sup>b</sup> 1.609(2) <sup>c</sup>	1.840(5), <sup>b</sup> 1.594(4) <sup>c</sup>	1.855(13)	1.825(6)
Bond Angles (deg)								
A-P-A (A = C, O) (av)	101.7(4)	103.8(3)	101.2(1)	104.7(2)	102.2(1), <sup>b</sup> 100.3(1) <sup>c</sup>	103.1(2), <sup>b</sup> 102.6(2) <sup>c</sup>	102.6(4)	104.6(2)
Rh-N-X (X = N, CMe)	123.6(5)	121.7(3)	128.4(2)	126.7(2)	127.0(2) <sup>b</sup>	124.7(3) <sup>b</sup>	130.5(10)	123.7(3)
	120.7(5)			126.5(3)	124.0(2) <sup>c</sup>	122.8(3) <sup>c</sup>	130.0(10)	125.0(3)
	125.9(5)	125.6(3)	121.8(2)	121.3(3)	123.7(2) <sup>c</sup>	123.0(3) <sup>c</sup>	123.6(10)	126.7(3)
	128.0(5)			121.0(3)	126.5(2) <sup>b</sup>	126.2(3) <sup>b</sup>	123.7(10)	128.0(3)
N-X-N (X = N, CMe)	119.8(6)	119.3(4)	120.1(3)	118.5(3)	119.7(3)	119.7(3)	119.7(12)	116.3(4)
	119.8(7)			119.9(4)	119.4(3)	118.5(4)	118.1(12)	116.2(4)
Torsion Angles (deg)								
P-Rh...Rh-C	23.7(3), 24.4(3)	18.2(3)	15.8(2)	17.9(1), 16.2(1)	15.3(1), <sup>b</sup> 18.0(1) <sup>c</sup>	13.9(2), <sup>b</sup> 15.7(2) <sup>c</sup>	22.2(5), 20.2(5)	16.5(2), 17.9(2)
N-Rh...Rh-N	24.9(2), 25.6(2)	22.0(3)	18.6(2)	18.8(1), 16.6(1)	18.7(1), <sup>b</sup> 19.8(1) <sup>c</sup>	18.6(1), <sup>b</sup> 18.7(1) <sup>c</sup>	21.2(6), 18.9(6)	21.5(3), 17.6(3)

<sup>a</sup> Estimated standard deviations (derived from crystallographic least-squares refinement for individual dimensions) in the least significant digit are given in parentheses, here and throughout this paper. <sup>b</sup> Dimensions for the (N)<sub>2</sub>Rh(CO)(PPh<sub>3</sub>) unit. <sup>c</sup> Dimensions for the (N)<sub>2</sub>Rh(CO){P(OPh)<sub>3</sub>} unit.

**Table 9.** Interplane and Staggering Angles<sup>a</sup>


compd	[Rh <sub>2</sub> ] <sup>2+</sup>		[Rh <sub>2</sub> ] <sup>3+</sup>		ref
	2β	2γ	2β	2γ	
1/1 <sup>+</sup>	40.4	25	32.9	20	this work
2/2 <sup>+</sup>	30.3	17	24.2	17	this work
3/3 <sup>+</sup>	31.5	18	26.9	17	this work
4/4 <sup>+</sup>	40.8	20	31.3	20	11e
6/6 <sup>+</sup>	0	0	ca. 0	ca. 0	12b
9/9 <sup>+</sup>	0	26	ca. 0	ca. 26	12e
11/11 <sup>+</sup>	57.1	36 <sup>b</sup>	ca. 50	ca. 36	12d
12/12 <sup>+</sup>	49.0	31	44.3	30	12c
16/16 <sup>+</sup>	80.7	0 <sup>c</sup>	ca. 70	ca. 0	10d

<sup>a</sup> The angle 2β (deg) is the angle between the mean planes defined by the rhodium atom and the four equatorial ligand atoms (in the cases of **11**, **12**, **12**<sup>+</sup>, and **13** the position of the olefin ligands was taken as the midpoint of the C=C bond); the angle 2γ (deg) is the average of the four torsion angles defined by L, Rh, Rh, L' (L, L' = CO or PR<sub>3</sub>) (see diagram). <sup>b</sup> Data for the iridium analogue [Ir<sub>2</sub>(μ-mhp)<sub>2</sub>(COD)<sub>2</sub>]. <sup>c</sup> Data for the pyrazolate analogue [Rh<sub>2</sub>(μ-pz)<sub>2</sub>(COD)<sub>2</sub>].

large part localized at the Rh<sub>2</sub> core of these complexes and the dimetal center changing from [Rh<sub>2</sub>]<sup>2+</sup> to [Rh<sub>2</sub>]<sup>3+</sup>. Furthermore it seems likely that an orbital of metal-metal antibonding character is depopulated in the process. In order to probe the electronic structure and assist in understanding the structural and ESR spectroscopic characteristics of these dirhodium species, we have carried out extended Hückel molecular orbital (eHMO) calculations<sup>19</sup> on a variety of models for complexes **1**–**5**. Model complexes {[Rh(H)<sub>2</sub>(CO)<sub>2</sub>]<sub>2</sub>}<sup>2-</sup> **14** and [Rh<sub>2</sub>(CO)<sub>4</sub>(μ-HNNNH)<sub>2</sub>] **15** were studied in most detail. In all cases the geometries used for **14** and **15** had all intraligand bond angles at rhodium = 90° or 180°, Rh-C-O = 180°, and N-N-N and N-N-H = 120.0° in **15**, with bond lengths (Å) Rh-H = 1.60, Rh-Rh = 2.96 or 2.70, Rh-C(O) = 1.808, C-O = 1.152, N-N = 1.300, and N-H

= 1.00. Hückel parameters were taken from the literature.<sup>20</sup> Torsion angles β and γ (see Table 9) were varied across the range 0–30° to assess their effects on the electronic structures of the complexes.

Initial calculations indicated that simple model complexes **14** and **15** provided reasonably accurate models in that they gave orbital energies and characteristics close to those for more complex molecules in which less symmetry was imposed and geometries were taken from crystal structure analyses. Furthermore, in terms of the HOMO characteristics, the results of these calculations were in reasonable agreement with those on related systems using more quantitatively reliable levels of theory.<sup>21</sup> Some of the results of our calculations are summarized in Table 10 which reports details for the Rh<sub>2</sub><sup>3+</sup> complex **14**<sup>+</sup> with Rh...Rh distance set to 2.70 Å and the ligands eclipsed (*i.e.* γ = 0°). Conclusions for **15** were qualitatively identical to those for **14**.

As predicted from the structural observations, the HOMO of the [Rh<sub>2</sub>]<sup>2+</sup> species **14** and **15** (and hence the SOMO (singly occupied molecular orbital) of the [Rh<sub>2</sub>]<sup>3+</sup> species **14**<sup>+</sup> and **15**<sup>+</sup>) in all geometries is largely an out of phase combination of rhodium d<sub>z</sub> orbitals (z perpendicular to the coordination plane, *i.e.* in the local axis system). The HOMO/SOMO therefore has Rh-Rh σ\* character when the dihedral, interplane angle 2β = 0°. This is in accord with the previous calculations<sup>21</sup> on related [Rh<sub>2</sub>L<sub>8</sub>]<sup>4+</sup> species (where the coordination planes are usually parallel) for which this orbital is the LUMO. Depopulation of the HOMO (*i.e.* in **14**<sup>+</sup> as compared with **14**) causes a substantial rise in the Rh...Rh overlap population as expected (from 0.096 to 0.151 at Rh...Rh = 2.70 Å). Increasing β from 0 to 20° causes a small decrease in the energy of this orbital, as the interaction becomes more π\* in character (see Figure 4). At values of β > 25° the SOMO energy for **14**<sup>+</sup> begins to rise as H...H σ\* character starts to mix in. The calculated total one-electron energy also shows a decline initially, reaching a minimum at β = ca. 10°. In concert with these changes the net Rh...Rh overlap (for **14**<sup>+</sup> at Rh...Rh = 2.70 Å) rises from 0.151 at β = 0 to 0.175 at β = 10°. These observations are in line with a decrease in the antibonding contribution from the SOMO. The subsequent (*i.e.* for β > 10°) rise in total energy and fall in Rh...Rh overlap is due to previously π\* interactions (*i.e.* between Rh d<sub>zx</sub>), which become increasingly σ\* in character as β rises, and, more importantly, because of destabilising four-electron interactions between the H ligands in

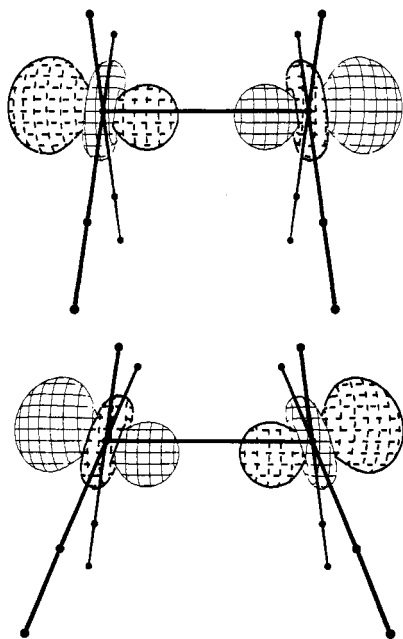
(19) (a) Hoffmann, R. *J. Chem. Phys.* **1963**, *39*, 1397–1412. (b) Howell, J.; Rossi, A.; Wallace, D.; Harak, I. K.; Hoffman, R. *QCPE* **1977**, *10*, 344. (c) Mealli, C.; Proserpio, D. M. *J. Chem. Educ.* **1990**, *67*, 399–402.

(20) Hoffmann, R.; Minot, C.; Gray, H. B. *J. Am. Chem. Soc.* **1984**, *106*, 2001–2005.

(21) Cotton, F. A.; Feng, X. *Inorg. Chem.* **1989**, *28*, 1180–1183.

**Table 10.** Summary of Results of EHMO Calculations on  $[\{\text{Rh}(\text{H})_2(\text{CO})_2\}_2]^-$  ( $14^+$ ) with  $\text{Rh}\cdots\text{Rh} = 2.70 \text{ \AA}$  and  $\gamma = 0^\circ$ 

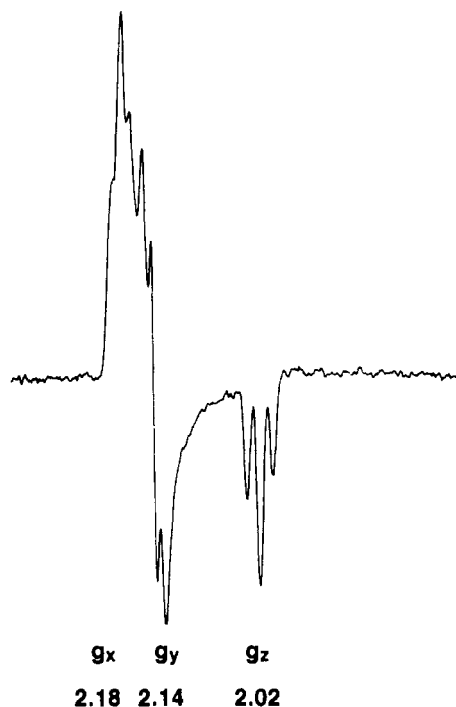
	$\beta$ (deg)						
	0	5	10	15	20	25	30
tot. energy (eV), rel to $\beta = 0$	0.00	-0.24	-0.30	-0.23	-0.02	0.38	0.99
SOMO energy (eV)	-10.649	-10.670	-10.694	-10.721	-10.721	-10.744	-10.727
Rh 4d contribn to SOMO	0.72	0.71	0.70	0.68	0.64	0.60	0.50
Rh 5s contribn to SOMO	0.10	0.10	0.11	0.11	0.11	0.12	0.12
Rh $\cdots$ Rh reduced overlap population	0.151	0.167	0.175	0.173	0.162	0.141	0.109

**Figure 4.** CACAO<sup>19c</sup> plots of the SOMO of  $[\{\text{RhH}_2(\text{CO})_2\}_2]^-$  ( $14^+$ ) as derived by EHMO calculations (a, top) for  $\beta = 0^\circ$  and (b, bottom) for  $\beta = 15^\circ$ .

$14^+$ . These latter interactions are of course reduced in cases where  $\gamma \neq 0^\circ$  and for the real complexes in which bridging ligands replace the hydrides of the model. Thus these observations are consistent with the observed structures of the complexes  $1^+$ – $4^+$  which have  $\beta$  ca.  $15^\circ$ .

The orbital composition of the SOMO in  $14^+$  is somewhat dependent on  $\beta$  but essentially invariant as a function of the torsion angle  $\gamma$ . The calculated amount of rhodium 4d and 5s character in the SOMO changes only slightly with  $\beta$  in the range  $0$ – $20^\circ$ ; total contributions are 0.72 and 0.10, respectively ( $\beta = 0^\circ$ ), and 0.64 and 0.10 ( $\beta = 20^\circ$ ). At still higher values of  $\beta$  this orbital is increasingly delocalized on to the ligands and hence has less Rh character, but this effect is at least in part associated with the nature of the model system in which bridging ligands have been replaced with hydrides. As shown in Figure 4, the HOMO/SOMO is essentially anchored perpendicular to the local coordination plane at Rh and the 4d component is almost exclusively (>90%)  $d_{xz}$  throughout the range  $0 \leq \beta \leq 30^\circ$ . In addition to the Rh 5s and 4d components of the HOMO/SOMO we calculate a Rh 5p<sub>z</sub> component (total Rh 5p charge density 0.10) which rehybridizes the orbital so as to reduce the Rh $\cdots$ Rh antibonding character (see Figure 4). In addition at small values of  $\beta$  (< $10^\circ$ ) there is a perceptible (charge density ca. 0.04) mixing of  $d_{xz}$  into the HOMO in such a way as to rotate the rhodium orbitals very slightly off the Rh $\cdots$ Rh axis. This mixing disappears at higher values of  $\beta$ .

The HOMO in  $14$  is weakly Rh–H  $\sigma^*$  in character, in accord with the observation that its depopulation results in a decrease of the Rh– $\sigma$ -ligand bond distances. Finally we note that depopulation of this orbital will greatly reduce the barrier to attack of nucleophiles at the pseudo-axial site of the  $\text{Rh}_2$  fragment (*i.e.* *trans* to the Rh $\cdots$ Rh vector) by reducing the four-electron repulsion between the nucleophile lone pair and the pair of electrons in the HOMO.

**Figure 5.** ESR spectrum of  $3^+$  at 123 K, in  $\text{CH}_2\text{Cl}_2$ -thf (1:2).**Table 11.** ESR Parameters

radical	$g_x$	$g_y$	$g_z$	$A_x^a$	$A_y^a$	$A_z^a$
$1^+$	2.180	2.157	2.021	14.2	15.9	20.0
$2^+$	2.166	2.138	2.021	16.7	16.1	22.4
$3^+$	2.180	2.140	2.020	16.6	15.7	22.8
$4^+$	2.18	2.157	2.019			18.4
$5^+$	2.185	2.130	2.014	11.6	11.3	18.1
$6^+$	2.246	2.216	1.999	14	17	21
$7^+$	2.226	2.196	1.994	13	18	21
$8^+$	2.198	2.164	1.995			17
$9^+$	2.228	2.194	1.997			17
$10^+$	2.152	2.152	2.022			17
$11^+$	2.278	2.278	2.098			
$12^+$	2.249	2.214	2.080			
$13^+$	2.239	2.220	2.076			ca. 10
$16^{+b}$	2.24	2.24	2.13			17.9

<sup>a</sup> In units of  $10^{-4} \text{ cm}^{-1}$ ; directions correspond to  $g$ -matrix principal axes. <sup>b</sup> Reference 10b.

**Analysis of ESR Spectra.** Frozen solution spectra of the  $[\text{Rh}_2]^{3+}$  containing cations are approximately axial with  $g_x > g_y \gg g_z$ . In the spectra of  $1^+$ ,  $2^+$ ,  $3^+$ ,  $5^+$ ,  $6^+$ , and  $7^+$ , each of the three features is a 1:2:1 triplet due to hyperfine coupling of two equivalent  $^{103}\text{Rh}$  nuclei;<sup>22</sup> a representative spectrum, of  $3^+$ , is shown in Figure 5. On the basis of the line widths, an upper limit of about 5 G can be placed on the  $^{31}\text{P}$  and  $^{14}\text{N}$  couplings. The spectra of the other cations are less well resolved, particularly in the perpendicular region but, except for  $11^+$  and  $12^+$ , still show  $^{103}\text{Rh}$  hyperfine structure on the parallel feature; in the spectrum of  $11^+$  the  $g_x$  and  $g_y$  features are unresolved. ESR parameters are given in Table 11. These spectra are qualitatively similar to that previously

(22) Coupling to  $^{31}\text{P}$  or  $^{14}\text{N}$  can be ruled out on the grounds that the same triplet splitting is observed for complexes with 0, 2, or 4 ligand phosphorus or nitrogen atoms.

reported for  $[\text{Rh}_2(\mu\text{-dmpz})_2(\text{COD})_2]^+$  ( $16^+$ , dmpz = 3,5-dimethylpyrazolate)<sup>10b</sup> parameters for which are included in Table 11 for comparison.

The approximate  $C_{2v}$  symmetry of  $6^+ - 8^+$  and  $13^+$  requires that the principal axes of  $g$  correspond to the 2-fold axis and to normals to the reflection planes; thus, one of the axes must be along the Rh–Rh bond. The remaining radical cations have lower symmetry (at most  $C_2$ ). Nonetheless, it seems reasonable to assume that the Rh–Rh bond continues to correspond to one of the  $g$ -matrix principal axes. The X-ray structural data show that for  $1^+ - 4^+$  and  $12^+$  the rhodium coordination planes are tilted, relative to the  $C_2$  axis, by an angle  $\beta$ . The angle  $\beta$  for  $6$  and  $9$  is  $0^\circ$ , and we assume the cations  $6^+$  and  $9^+$  retain the exact face-to-face arrangement; for cations  $11^+$  and  $16^+$  values of  $\beta$  were estimated from those structurally determined for  $11$ ,  $16$ , and the redox pairs  $1/1^+ - 4/4^+$  and  $12/12^+$ . The rhodium coordination planes are also twisted relative to one another by the angle  $2\gamma$  as given in Table 9. When  $\gamma = 0$ , the Rh atoms lie in a plane of symmetry, requiring one of the  $A$ -matrix axes to lie along the normal (perpendicular to the Rh–Rh bond). In general, we assume that the major hyperfine axis, corresponding to  $A_{||}$ , lies along the normal to the local coordination plane so that the principal hyperfine axes are related to the  $g$ -matrix axes by the Euler angles,  $\pm\beta$  and  $\pm\gamma$ . In any case, the hyperfine components given in Table 11 are not the principal values of the hyperfine matrices.

**Interpretation of ESR Parameters.** For complexes  $6^+ - 9^+$ , where the coordination planes are parallel,  $g_z \approx g_e$ , suggesting that the metal 4d contribution to the SOMO is primarily  $d_{z^2}$ , consistent with characterization of the SOMO as the Rh–Rh  $\sigma^*$  MO. As the metal coordination planes are tilted,  $g_z$  becomes larger than  $g_e$ , as expected if the metal hybrid contribution to the SOMO changes with angle, incorporating  $d_{xz}$  or  $d_{yz}$  character, for example.

In order to make this notion quantitative, we assume that, for all radical cations in the series, the SOMO is an antibonding combination of metal  $d_{z^2}$  orbitals, where the atomic orbitals are defined in the local coordinate systems with the  $z$ -axes normal to the coordination planes,

$$|\text{SOMO}\rangle = c_0 \chi_{z^2}^- + \dots \quad (1)$$

where the functions such as

$$\chi_{z^2}^\pm = \frac{1}{\sqrt{2}}(|z^2\rangle_1 \pm |z^2\rangle_2) \quad (2a)$$

$$\phi_{z^2}^\pm = \frac{1}{\sqrt{2}}(|z^2\rangle_1 \pm |z^2\rangle_2) \quad (2b)$$

are symmetry-adapted combinations written in the local and  $g$ -matrix coordinate systems, respectively. Transforming eq 1 into the  $g$ -matrix coordinate system by rotation of the local axes of Rh(1) through the Euler angles  $\beta$  and  $\gamma$ , and those of Rh(2) through angles  $-\beta$  and  $-\gamma$ , we have

$$|\text{SOMO}\rangle = c_0 \left[ \frac{1}{2}(3 \cos^2 \beta - 1) \phi_{z^2}^- - \sqrt{3} \sin \beta \cos \beta (\cos \gamma \phi_{xz}^+ + \sin \gamma \phi_{yz}^-) + \frac{\sqrt{3}}{2} \sin^2 \beta (\cos 2\gamma \phi_{x^2-y^2}^- + \sin 2\gamma \phi_{xy}^+) \right] + \dots \quad (3)$$

Thus, for small  $\gamma$ , the rhodium contributions to the SOMO may be regarded as  $d_{z^2} - d_{xz} - d_{x^2-y^2}$  hybrids with composition as shown in Figure 6. Applying eq 3 of ref 6b, we obtain

$$\Delta g_x = 3c_0^2 (\delta_{yz}^+ \cos^2 \beta \cos^2 \gamma + \delta_{xz}^- \sin^2 \gamma) \quad (4a)$$

$$\Delta g_y = 3c_0^2 (\delta_{yz}^+ \cos^2 \beta \sin^2 \gamma + \delta_{xz}^- \cos^2 \gamma) \quad (4b)$$

$$\Delta g_z = 3c_0^2 \delta_{yz}^+ \sin^2 \beta \quad (4c)$$

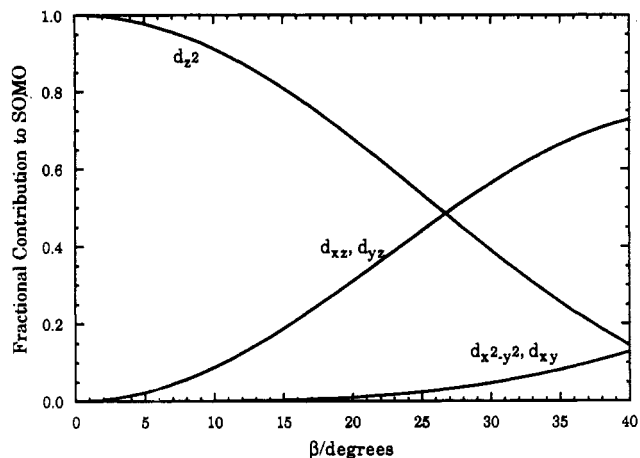


**Figure 6.** Hybridization of the SOMO in the  $g$ -tensor coordinate system as a function of  $\beta$ , half the angle between coordination planes for the  $[\text{Rh}_2]^{3+}$  complexes.

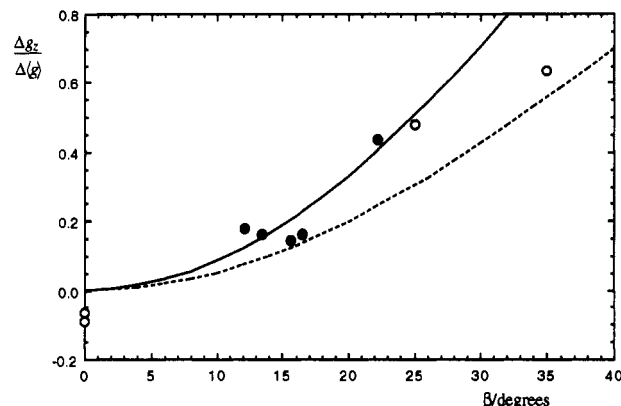


**Figure 7.**  $\Delta g_z / \Delta(g)$  as a function of  $\beta$ , half the angle between coordination planes for  $[\text{Rh}_2]^{3+}$  complexes. The solid line is a least-squares fit of the experimental data to eq 6b. The open circles represent data not included in the least-squares fit; for these  $\beta$  was estimated from the angle for the corresponding  $[\text{Rh}_2]^{2+}$  complex. The dashed line corresponds to  $R = 1.29$ .

where  $\Delta g_i = g_i - g_e$  and the parameters  $\delta_i^\pm$  are given by eq 5. In eq 5,  $\zeta_{\text{Rh}}$  is the spin-orbit coupling constant and  $c_{ik}^\pm$  is the LCAO coefficient of  $\chi_i^\pm$  in the  $k$ th molecular orbital with energy  $E_k$ .

$$\delta_i^\pm = 2\zeta_{\text{Rh}} \sum_{k \neq 0} \frac{(c_{ik}^\pm)^2}{E_0 - E_k} \quad (5)$$

Equations 4 may be rearranged to predict more explicitly the departure from axial symmetry and the shift of  $g_z$  from the free electron value.

$$\frac{g_x - g_y}{\Delta(g)} = \frac{3(R \cos^2 \beta - 1) \cos 2\gamma}{1 + R} \quad (6a)$$

$$\frac{\Delta g_z}{\Delta(g)} = \frac{3R}{1 + R} \sin^2 \beta \quad (6b)$$

where  $R = \delta_{yz}^+ / \delta_{xz}^-$ . Using  $1^+ - 4^+$ ,  $6^+$ ,  $9^+$ , and  $12^+$ , for which the perpendicular feature is resolved into  $x$ - and  $y$ -components and structural data are available, eq 6a leads to  $R = 1.3 \pm 0.1$  and  $3R/(1 + R) = 1.7 \pm 0.1$ .<sup>23</sup> A plot of  $\Delta g_z / \Delta(g)$  vs  $\beta$ , shown in Figure 7, shows a good correlation with a least-squares slope,  $3R/(1 + R) = 2.2 \pm 0.2$  ( $R = 2.8 \pm 0.4$ ), in reasonable agreement with the value obtained using eq 6a. The plot of Figure 7 also

(23) The opposite assignments of  $g_x$  and  $g_y$  lead to a poorer fit to both eqs 6a and 6b.

provides a means of roughly estimating the angle of coordination plane tilt, given a value of  $g_z$  for [Rh<sub>2</sub>]<sup>3+</sup> complexes of unknown structure. Thus, for example,  $g_z$  for 5<sup>+</sup> is significantly closer to  $g_x$  than for 1<sup>+</sup>–4<sup>+</sup>, suggesting a smaller tilt angle, consistent with the presence of a bridging dpmm ligand.

Uncertainties in the experimental parameters and the large contributions of spin–orbit coupling preclude a detailed analysis of the <sup>103</sup>Rh hyperfine coupling, but we can obtain order-of-magnitude estimates. In the  $g$ -matrix coordinate system, the <sup>103</sup>Rh dipolar hyperfine matrices are not diagonal, but the observed splittings in the frozen-solution spectra correspond, at least approximately, to the  $x$ -,  $y$ -, and  $z$ -axes in the  $g$ -matrix coordinate system. Computing the dipolar and spin–orbit coupling contributions to the  $z$ -component of the hyperfine matrix in the  $g$ -tensor coordinate system, we obtain the following expressions:<sup>6b,24</sup>

$$A_{zz} \cong A_s + \frac{Pc_0^2}{7}[1 + 3 \cos 2\beta] + P[\Delta g_z - 1/14 \Delta g_x] \quad (7a)$$

$$\langle A \rangle = A_s + \frac{P}{3}[\Delta g_x + \Delta g_y + \Delta g_z] \quad (7b)$$

where  $P = -40.4 \times 10^{-4} \text{ cm}^{-1}$  is the dipolar coupling parameter<sup>25</sup> and

$$A_s = Q_d \rho_{4d} + Q_s \rho_{5s} \quad (8)$$

is the isotropic coupling resulting from polarization of inner-shell  $s$ -orbitals by rhodium 4d spin density ( $Q_d \approx 32 \times 10^{-4} \text{ cm}^{-1}$ )<sup>26</sup> and from the direct contribution of rhodium 5s spin density ( $Q_s = -410 \times 10^{-4} \text{ cm}^{-1}$ ).<sup>25</sup>

The signs of the components of  $A$  are indeterminate, but the assumption of a  $d_{z^2}$ -based SOMO is consistent only if all components are negative. The assignments of the  $z$ -component of  $g$  and  $A$  are unambiguous in all cases, so that  $A_{zz} - \langle A \rangle$  can be computed and used to estimate the rhodium 4d spin densities using experimental values of  $\beta$ . Equations 7b and 8 then can be used to compute the 5s contribution. For 1<sup>+</sup>, 2<sup>+</sup>, 3<sup>+</sup>, 5<sup>+</sup>, 6<sup>+</sup>, 7<sup>+</sup>,

and 9<sup>+</sup>, we obtain  $\rho_{4d} \approx 0.3$ –0.5 and  $\rho_{5s} \approx 0.05$ –0.07 for each rhodium atom, consistent with the EHMO estimates for 14<sup>+</sup>.

## Conclusions

The studies reported in this paper have sought to establish the geometric and electronic structure of ligand-bridged dirhodium complexes containing the [Rh<sub>2</sub>]<sup>3+</sup> core. The geometric features of this class of complex are firmly established by crystal structure analyses of salts of three such complexes 1<sup>+</sup>–3<sup>+</sup> and their reduced neutral counterparts. The complexes which have only two bridging ligands adopt a structure in which the RhL<sub>4</sub> coordination planes are splayed apart. Taken together with the tetrabridged species previously studied, interplanar angles ( $2\beta$ ) are observed in the range 0–80°. In the [Rh<sub>2</sub>]<sup>3+</sup> form the Rh...Rh distances are substantially shorter [by between 0.147(2) and 0.262(4) Å for 1<sup>+</sup>–4<sup>+</sup>] and the interplanar angles ( $2\beta$ ) smaller than in their reduced [Rh<sub>2</sub>]<sup>2+</sup> counterparts. These and other geometrical changes indicate that the SOMO in the cations is largely metal-based and metal–metal  $\sigma^*$  in character. This conclusion is shown to be in full accord with eHMO calculations, which provide estimates of the orbital composition of the SOMO and suggest that the coordination planes are splayed in order to reduce the  $\sigma^*$  character of the Rh...Rh interaction. Finally these estimates of orbital composition are shown to be in good agreement with analyses of the ESR spectra of the [Rh<sub>2</sub>]<sup>3+</sup> complexes. The consistency between the three strands of this work lends particular force to the conclusions concerning the electronic structure of the complexed [Rh<sub>2</sub>]<sup>3+</sup> unit.

**Acknowledgment.** We thank the SERC for a Studentship (to K.E.R.) and a Postdoctoral Research Associateship (to G.G.H.), the NSF for financial support (Grant CHE-8722843, to K.R.M.), Johnson Matthey for a generous loan of rhodium salts, and the Royal Society and the Consiglio Nazionale delle Ricerche (CNR) of Italy for an exchange grant. We also thank Mr. Thomas Brauns for some initial calculations and pay tribute to the part played by Mr. C. J. Finn and Dr. M. J. Freeman in the earlier stages of this work (see ref 11e).

**Supplementary Material Available:** Tables of structure determination data, complete atomic positional and thermal parameters, anisotropic thermal parameters, and bond distances and angles (29 pages). Ordering information is given on any current masthead page.

(24) Peake, B. M.; Rieger, P. H.; Robinson, B. H.; Simpson, J. *J. Am. Chem. Soc.* **1980**, *102*, 156–163.

(25) Morton, J. S.; Preston, K. F. *J. Magn. Reson.* **1978**, *30*, 577–582.

(26) Muniz, R. P. A.; Vugman, N. V.; Danon, J. *J. Chem. Phys.* **1971**, *54*, 1284–1288.